

Dear Editor of Geoscientific Model Development,

We have modified the manuscript according to the remaining comments and queries from the two anonymous reviewers. The main points that were modified concern the inclusion into the main text of a part of the information contained in the supplementary materials and clarification of some misleading information. To fulfill these recommendations, we have:

- 1) Moved Figure 4 of the Supplement into Section 4.2.2 or 4.2.3 according to the referee suggestion. This latter presents sensitivity of the sea-ice model to coupling frequency. Although not central in the study, this information is valuable to track change in skill of the present model (CNRM-ESM1) compared to the previous version (CNRM-CM5 and CNRM-CM5.2).
- 2) Detailed how the water conservation has been improved in the current with the respect to the previous model versions.
- 3) Given some details on carbon cycle components (e.g., the implicit nitrogen limitation used in the ISBA land carbon cycle module, redfield ratio in the carbon pools simulated in the PISCES marine biogeochemical model)
- 4) Included further evaluation diagnostics in the supplementary materials (Figure comparing skill of CNRM-ESM1 versus CNRM-CM5.2) to support between-model comparison.
- 5) Included intercomparison diagnostics following Anav et al. (2013) to strengthen the evaluation of CNRM-ESM1 and to present how it compares with other IPCC-class Earth system models.

Please find a detailed response to each questions/comments point by point below in [blue](#) (text fragments are [in blue italics](#)).

Reviewer # 1:

The authors present the development and a first evaluation of the CNRM earth system model, which evolved from the climate model CNRM-CM5 by coupling modules for the land and ocean carbon cycle to the model. They evaluate the main physical drivers of the land and ocean carbon cycle and compare these results to the previous model version. A number of ecosystem parameters, biogeochemical tracers, and carbon fluxes are evaluated against observation based estimates. The paper is of high scientific relevance for the earth system modelling community and definitely within the scope of the journal. The model-model and model-data comparisons are sound and the paper is overall well written. There are, however, a number of issues listed below that should be addressed by the authors. I recommend to accept the manuscript for publication in GMD after these minor revisions have been addressed by the authors.

General comments:

Comment 1: The authors find a quite large sensitivity of sea ice area to the coupling time step of the model (24h vs. 6h), but they somewhat hide this result in the supplement. Since this issue is mentioned several times in the manuscript, I suggest moving Figure 4 of the Supplement into Section 4.2.2 or 4.2.3 and discussing it there. Also, a discussion as to why the coupling time step causes these differences would certainly be of interest for the audience (although I see that this could be beyond the scope of this model description).

[We agree with the referee. Please see responses to comment 1 and 2 below.](#)

Comment 2: In 4.2.2 there is a discussion about deep convection in the model and the fact that CNRM-ESM1 simulates open ocean polynyas, but not in the region where the so-called wedell polynya was observed in 1974-1976. CNRM-CM5 in contrast simulated polynyas in the wedell sea, and the authors state that "The use of GELATO6 in CNRM-ESM1 compared to GELATO5 in CNRM-CM5 in addition to the change in coupling frequency might be at the origin of this model-data disagreement."

While it is interesting that open ocean polynyas have been observed and are not only seen in model simulations, the number of occurrences is a bit low to call this a "model-data disagreement" in my opinion. Is there any evidence that the difference in location is due to the different version of the ice model and/or the timestep? Isn't there a couple of other possible reasons in the model set-up? Altogether I find this paragraph on polynyas a bit too vague for a model evaluation paper, and I would suggest either deleting this discussion from the manuscript or go much more into the details as to why the location of polynyas is where it is in the different model versions (but this might as well be beyond the scope of this model description).

[We agree with the referee on both these comments.](#)

[This point is not central in the paper since it could be developed and further analyzed in another study, focused on the ocean and the sea ice. However, we have chosen to present the impact of the coupling frequency on sea-ice distribution to track changes in skill between the various CNRM models. In the present model, the representation of the sea](#)

ice has been degraded with respect to the previous model version.

That said, we agree with the referee on the fact we have brought information that is not in the scope of the current paper, e.g., impact of the open ocean polynia or the impact on the deep ocean ventilation. Therefore, we have removed the above-mentioned paragraph and presenting the Figure S4 in the main text as an evaluation material to explain the difference in skill of CNRM-ESM1 compared to CNRM-CM5.

Comment 3: p 5696, l 14-15: "...the model-data mismatch is likely related to the decision of Takahashi et al. (2010) to exclude observations from El Niño years from their analysis [...] This hypothesis is validated when comparing model results against recent data products derived from statistical Monte-Carlo Markov Chain or Neural Network gapfilling methods (Landschützer et al., 2014; Majkut et al., 2014)."

If the comparison with the latter data products gives better or different results, these should be presented here. Why compare to a data product with a known bias and then discuss that if we would compare to another available data product results would look better?

The reviewer is right but we have preferred to keep 'direct' observations from Takahashi et al. (2010) rather than observation-derived estimate like that of Landschützer et al., 2014.

Nonetheless, we have provided Figure R1 as comparison in the supplementary materials.

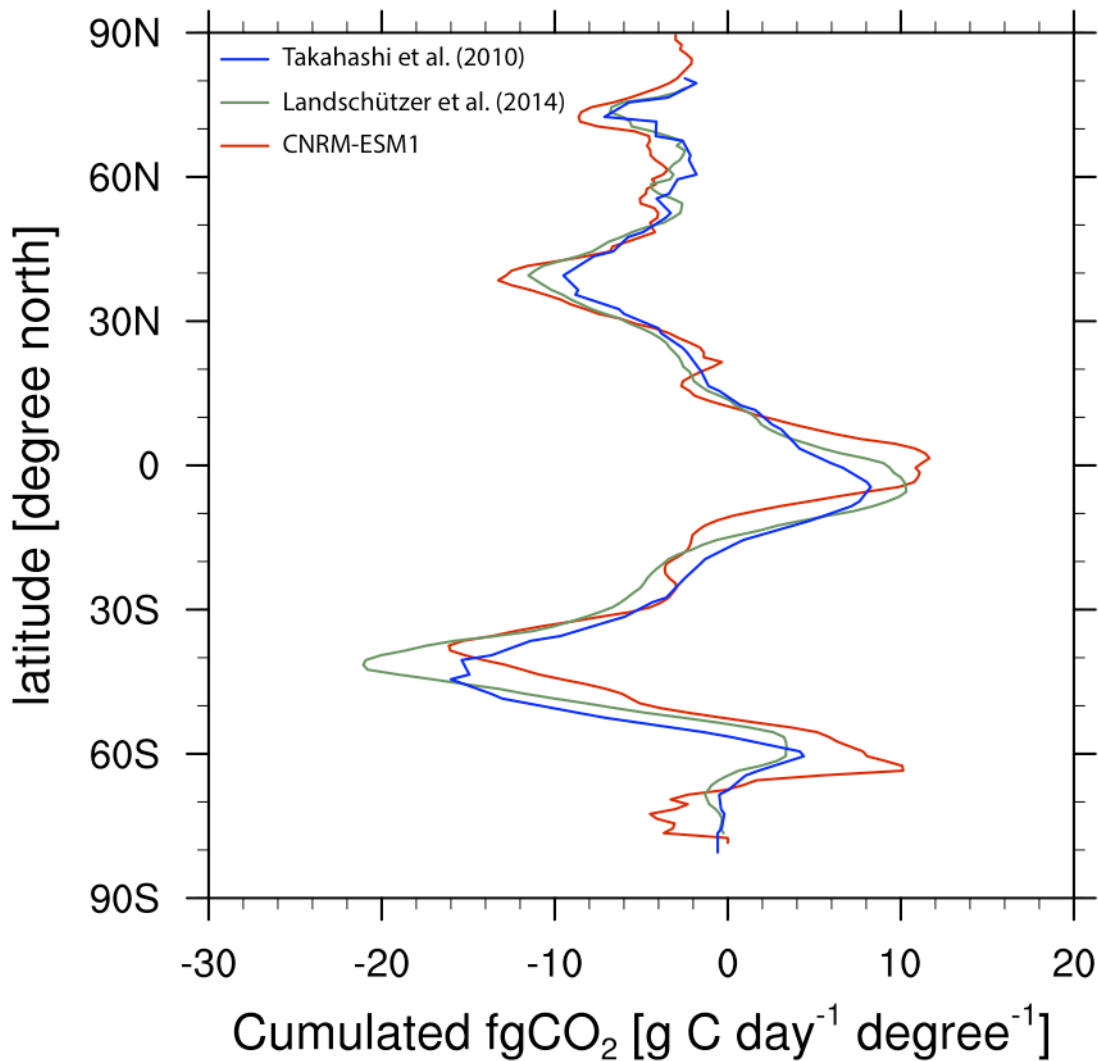


Figure R1: Zonally-cumulated ocean carbon fluxes (fgCO_2) averaged over 1986-2005 from observation-derived estimates and as simulated by CNRM-ESM1. Observation-derived estimates from Takahashi et al. (2010) and Landschützer et al. (2014) are represented with blue and green solid lines, respectively. Result from CNRM-ESM1 is given with a solid red line.

Comment 4: Summary, p 5702, l 5-8: "This change is attributed to [...] a higher coupling frequency that induces a stronger northward flow of deep water masses from the Southern Ocean." In the manuscript, the authors do not provide any evidence or model sensitivity tests to support this hypothesis. Unless they do so in a revised version of the manuscript, I suggest deleting the statement on the coupling frequency here.

We apologize for this lack of clarity. Some results and discussions have been provided in the section 4-2-2 of the submitted version of the manuscript:

"In the Southern Ocean, the flow of Antarctic bottom water (AABW) is about 11.6 ± 1 Sv

in CNRM-ESM1 averaged over the 1850-2005 period. This flow of AABW is in agreement with the deep flow of waters compared to the observed estimate of 10 ± 2 Sv (Orsi et al., 1999). Consequently, the flow of deep water masses in CNRM-ESM1 is stronger than that of CNRM-CM5 (Séférian et al., 2013; Voldoire et al., 2013)."

However, we have omitted to provide evidence of this improvement in order to compare our results to previous model version.

The text has been replaced by:

"This flow of AABW is in agreement with the deep flow of waters compared to the observed estimate of 10 ± 2 Sv (Orsi et al., 1999). Consequently, the flow of deep water masses in CNRM-ESM1 has been improved in regards that of CNRM-CM5 which ranges between 3.4 and 6.2 Sv over the same period (Séférian et al., 2013; Voldoire et al., 2013)."

In the summary, we have followed referee suggestion and reword the statement on the Southern Ocean circulation as follows.

Submitted:

"This change is attributed to improved water conservation in the ocean-sea ice model as well as a higher coupling frequency that induces a stronger northward flow of deep water masses from the Southern ocean."

Revised:

"This change is attributed to a stronger northward flow of deep water masses from the Southern ocean."

Specific comments:

In the abstract, please state to which time period the uptake values (2.2PgCyr⁻¹ land sink, 1.7PgCyr⁻¹ ocean sink) refer to.

Done and acknowledged

p 5673, l 6-10: "The models of this class ... primarily through their contribution to the concentration- and emission-driven experiments that compose CMIP5." I don't really understand what the authors want to say here. The really new point with ESMs is that we can run emission driven (something that traditional climate models cannot)

We agree with the reviewer but ESM including carbon cycle components enables biophysical interactions like the impact of rising CO₂ on evapotranspiration or the shading of ocean biota on light transfer and hence heat trapping. As such, ESM components, even under concentration-driven scenario, can generate feedback that traditional climate models do not simulate. Besides, ESM components have been investigated in terms of impacts like ocean acidification, variability etc... in various IPCC reports based on working groups 1 and 2.

Therefore, we chose to keep the sentence as it is.

p 5673, l 18: Please consider replacing "ensemble" by something else. "Ensemble" should

be reserved for different realisations of model runs of the same model, which the authors do not mean here, as far as I understand.

Done and acknowledged

p 5680, l 25-29: The nitrogen limitation of the Land BGC model is mentioned and a reference is given (Calvet et al.2008). Nitrogen limitation is a critical point in ESM simulations, and CMIP5 has shown that including it can potentially alter the reaction of land carbon uptake to enhanced CO₂ and climate change dramatically. Therefore, I think it would be good to provide a brief summary of how the nitrogen limitation is implemented in the CNRM-ESM.

We agree with the reviewer. We have amended the text as follows.

Submitted:

“It results that nitrogen dilution occurs as soon as the increase in total biomass of a plant under rising CO₂ relative to growth under ambient CO₂ is greater than the corresponding increase in total nitrogen.”

Revised:

“ISBA uses an implicit nitrogen limitation parameterization which is based on the meta-analysis of leaf nitrogen measurement under CO₂ enrichment condition (Yin et al., 2002). This simple implicit nitrogen limitation is based on the nitrogen dilution hypothesis, which assumes that internal nitrogen content of a plant decrease under rising CO₂ due to the accumulation of non-structural carbohydrates. It results that nitrogen dilution occurs as soon as the increase in total biomass of a plant under rising CO₂ relative to growth under ambient CO₂ is greater than the corresponding increase in total nitrogen. In current version of ISBA, a linear decrease between specific leaf area index and nitrogen to carbon ratio in leaves is used to mimic this mechanism (Calvet et al., 2008), and hence to limit the net assimilation of atmospheric CO₂.”

This simple implicit nitrogen limitation is used to relate internal concentration of nitrogen to biomass and to limit the net assimilation of atmospheric CO₂.

p 5682, l 21-22: "Only the internal concentrations of iron, silicon and calcite inside the sinking particles are prognostically simulated." I think this can be misleading: The amount of carbon transported down by sinking is also prognostically simulated, right? Only the ration C:P and C:N is fixed. Please clarify.

The information is given above in the main text:

“The ratios between carbon, nitrate and phosphate are kept constant to the values proposed by (Takahashi et al., 1985) in all living and nonliving pools of organic matter.”
We chose to keep the sentence as it is.

p 5683, l 2-5: Nitrogen fixation is mentioned, ("... nitrogen fixation should balance...") but it remains unclear how it is implemented. Could the authors please clarify.

We have clarified this sentence as follows:

“Importantly, to ensure conservation of nitrogen in the ocean, annual total nitrogen fixation is adjusted to balance losses from denitrification following (Lipschultz et al., 1990; Middelburg et al., 1996; Soetaert et al., 2000).. For the other macronutrients, alkalinity and organic carbon, the conservation is ensured by tuning the sedimental loss to the total external input from rivers and dust. Therefore, carbon and nitrogen cycles are decoupled to a certain degree.”

Section 3.1: In my opinion "Equilibrium strategy" is not a very good title for this section. The authors describe the spin-up of the model here, so "Spin-up strategy" or just "Model Spin-up" would be more suitable perhaps. Also, in line 7 a 320 year online spin-up is mentioned. Then towards the end of the section there is "an online adjustment ... for 400 years". Is this something different? Or is this the same as 320 years, but one of both is a typo? Please clarify, and (if the same) consider mentioning the online spin-up only once in this section.

We have changed the title as suggested by the referee
Besides, the review is right, the word 'online' (by opposition with offline) is not useful here because all the ESM components were spun-up within a coupled ESM.

p 5685 l 16: "...performed with the NCAR model (Ammann et al.,2007)." The "NCAR model" should be CCSM.

Done and acknowledged

p 5685 l 24: "...20th century reconstruction of the NCAR model (Ammann et al.,2003)." The "NCAR model" would be the CCSM, but in Ammann et al.(2003) they don't use CCSM or another model developed by NCAR. Please make sure that the model name and reference are correct.

We apologize for this misleading information. Both preindustrial and historical simulations rely on the reconstruction from Ammann et al., (2007) performed with the NCAR Community Climate System Model.

p 5687, l 4-6: I do not understand how the land C flux could be "explained by missing processes in ISBA such as the [...] riverine-induced carbon transport from land to oceans". A riverine transport could close the carbon cycle in the sense that it would transport the excess C taken up by land into the ocean eventually. This would still result in a positive land C-flux (but the land pool size would be constant in equilibrium which cannot be the case in the current model setup).

The Figure represents the NBP, which is decomposed as follows:

$$\text{NBP} = \text{GPP} - \text{TER} - \text{Fire} - \text{VOC} - \text{DC} - \text{LUC} - \text{CH}$$

With each flux >0

In the version of ISBA used in CNRM-ESM1, $\text{NBP} = \text{GPP} - \text{TER}$.

Therefore, missing processes like Fire, weathering or land-use land-cover change lead to overestimate NBP.

p 5688 l 3-4: "...appears to amplify the global average cold bias of 0.8C (with biases of -0.7 and -1C in boreal winter and summer, respectively)" I do not understand these numbers: Are these the differences between CNRM-CM5 and CNRM-ESM? The ESM biases have already been state above? Please clarify.

We have clarified our statement as follows:

"Small deviations between CNRM-CM5 and CNRM-ESM1 mean state can be essentially attributed to the land carbon cycle, which appears to amplify the global average annual cold bias of 0.8°C (with seasonal differences between CNRM-ESM1 and CNRM-CM5 of -0.7°C and -1°C in boreal winter and summer, respectively)."

p 5688, l 20: "Summer PR is similar between the two models with non-significant changes in simulated values ($< 10^{-5}$ mm day⁻¹)." I find it difficult to believe that PR changes are that small between the two different models, particularly since during boreal winter bias is reduced by 0.014 mm day⁻¹. Please check and/or clarify.

We thank the referee for his/her thoughtful comments. We have amended the text for sake of clarity.

We have changed following statement accordingly.

Submitted:

"The mismatch between simulated and GPCP observed PR over continents is slightly improved during the boreal winter with a bias reduced by 0.014 mm day⁻¹ in CNRM-ESM1. Summer PR is similar between the two models with non-significant changes in simulated values ($< 10^{-5}$ mm day⁻¹) but their geographical patterns have been slightly degraded in CNRM-ESM1 compared to CNRM-CM5. Although weak, changes induced by the ISBA biophysical coupling slightly improve the representation of the seasonal cycle in PR over Northern mid-latitude continents by amplifying the seasonal maximum and shifting it from June in CNRM-CM5 to July in CNRM-ESM1 (supplementary materials)."

Revised:

"Although weak, changes induced by the ISBA biophysical coupling slightly affect the representation of the seasonal cycle in PR over the vegetated regions (Figure S1). These lead to improve the simulated PR in CNRM-ESM1 compared to CNRM-CM5 over some vegetated regions during the growing season (spring-summer). Between 30°N and 60°N, the averaged error in simulated PR compared to GPCP is reduced by 0.12 mm day⁻¹ in CNRM-ESM1 compared to that of CNRM-CM5. Over the tropics (30°S-30°N), simulated PR is also improved in CNRM-ESM1 compared to CNRM-CM5 but to a lesser extent with a reduction of the averaged error by 0.06 mm day⁻¹ with respect to GPCP. Although PR have been improved over some region, their geographical patterns have been degraded in CNRM-ESM1 compared to CNRM-CM5, especially during the winter."

Section 4.2.2, evaluation of MLD: The terms MLD_max and MLD_min are a bit

ambiguous. I guess it is not the real min and max over all model timesteps but rather the min and max of the mean over some period (probably monthly)? Is this time window comparable to the time resolution of the Sallee data? Also please consider to call the Sallee et al data "observation based estimate" or similar, not "observations" in the figure caption of Figure 7.

The reviewer is right both model and data are used with a monthly temporal frequency. The figure caption has been amended accordingly.

p 5693, l 8: "...but strongly overestimates the spatial variations of this field." From Figure 9 i read a standard deviation < 1 for MLD in both cases, which means that variability is underestimated compared to observations. Regarding Figure 9: Since the small symbols for seasonal values are there, they should be discussed (why are there two seasons where MLD is very different in the two models)?

We apologize for this misleading information.

Erroneous computations were performed for the mixed-layer depth at seasonal timescale. They are now performed accurately and Figure 9 has been updated accordingly. Besides, the referee is right. CNRM-ESM1 underestimates the depth of the seasonal mixed-layer depth. We have corrected this mistake accordingly.

p 5693, l 14-15: "...difference in simulated SSS between the two models can be attributed to the revised water conservation interface and erroneous distribution of sea- ice cover. Besides, changes in coupling frequency (i.e. 24 to 6 h) might be at the origin of differences in skills between the two models." I do not understand what the "revised water conservation interface" is. If this leads to important differences it must be at least briefly described Section 2. Is there any evidence that the coupling frequency changes the model skill in reproducing SSS?

Following referee remarks, we have modified this statement as follows.

Submitted:

"Since CNRM-CM5.1, the coupling between NEMO and GELATO has been revised in order to improve the conservation of water and salt."

Revised:

"Since CNRM-CM5.1, the coupling between NEMO and GELATO has been revised in order to improve the conservation of water and salt. In the previous model version, CNRM-CM5.1, there was a large drift in salinity (-0.011psu/century) and in sea level (-21 cm/century). These were caused by (1) the melting of land glaciers (other than Antarctic and Greenland) that was not routed to the ocean and (2) an erroneous coupling between sea-ice and ocean models. The coupling did not take into account the fact that sea ice is levitating over the ocean in this version of NEMO. Although not severe, it resulted in a loss of water in the model. These errors have been fixed in CNRM-CM5-2 and CNRM-ESM1 and hence reducing the residual drifts in salinity to +0.001psu/century and in sea level to +1.2cm/century."

p 5699, l 5: replace "climate change" with "climate forcing". The climate change is seen in the indices looked at, which react to a forcing.

Done and acknowledged

Figure 2: The text says, land carbon flux is 0.75 PgCyr-1. From the Figure I would guess that the number must be more around 1.25. So I assume that either the Figure axis or the number in the text is wrong. Please check.

The reviewer is right but we are comparing two different period:

Land sink is about 0.75 PgC y-1 over the preindustrial period in our model. This value has been computed from an average flux over 400-year long piControl simulation.

The land sink in the early 20th century is about 1.2 PgC y-1 (in 1901-1910). This value accounts for both low frequency fluctuations (in response to climate mode of variability) and to a lesser extent rising of atmospheric CO₂. This latter has risen by about 11 ppm from 1850 to 1901.

Technical corrections:

When referring to the supplement, could the authors please give the figure number, rather than just "(Supplement)".

Done and acknowledged

p 5675, l 3: acronym AOGCM not explained at first use

Done and acknowledged

p 5675, l 6: "...(ARPEGE-Climat, SURFEX, NEMO, GELATO, respectively)" this addition makes no sense without further explanation. Since all components are discussed below, I would just delete this.

Done and acknowledged

p 5675, l 8: "...was based on version 5.2. This version of the atmospheric code derives from cycle 37 of..." I think the authors mean their version 6.1, but as the sentence is constructed "This" refers to version 5.2. Please consider rephrasing to avoid confusion.

We agree with the referee. To avoid confusion, we have modified this sentence as follows.

Submitted:

"The atmospheric component is based on version 6.1 of the global spectral model ARPEGE-Climat whereas CNRM-CM5.1 was based on version 5.2. This version of the atmospheric code derives from cycle 37 of the ARPEGE-IFS (Integrated Forecast System) numerical weather prediction model developed jointly by Météo-France and the European Center for Medium-range Weather Forecast."

Revised:

“The atmospheric component is based on version 6.1 of the global spectral model ARPEGE-Climat which corresponds to an updated version of the atmospheric code used in CNRM-CM5.1. This updated version of the atmospheric code derives from cycle 37 of the ARPEGE-IFS (Integrated Forecast System) numerical weather prediction model developed jointly by Météo-France and the European Center for Medium-range Weather Forecast.”

p 5675, l 23-24: "The main difference from the CNRM-CM5.1 atmospheric model is the improved treatment of volcanic aerosols." But this is not a difference in ARPEGE, right? If so, please consider rephrasing something like "The interactive chemistry module already used in CNRM-CM5.1 has been updated with an improved..."

We apologize for this misleading statement.

Improvements concern only coefficients for the stratospheric chemistry module, not the atmospheric code. We have deleted this statement from the main text.

p 5678, l 1: "The coupling between the atmosphere and the surface models is implicit..." I do not understand what "implicit" should mean here. I guess, the land surface is a sub-model of the atmosphere (organised as a subroutine call)? Please reword this sentence.

We have amended this sentence as follows.

Submitted:

“The coupling between the atmosphere and the surface models is implicit and occurs every atmospheric timestep (i.e., 30 minutes) while the coupling between the atmosphere and the ocean models is handled by the OASIS coupler (Valcke, 2013) and occurs every 6 hours.”

Revised:

“In CNRM-ESM1, exchanges of momentum, water and energy between the atmosphere and the surface models occurs every atmospheric timestep (i.e., 30 minutes) because SURFEX is a submodel of the atmospheric code. The coupling between the atmosphere and the ocean models is handled by the OASIS coupler (Valcke, 2013) and occurs every 6 hours.”

p 5678, l21: "... the recommendations of the JPL-2003-25 report (Sander et al., 2006)." The "JPL-2003-25" is not helpful for the reader, consider rephrasing: "...the recommendations of Sander et al. (2006)." Please also correct the reference Sander et al. (2006) in the References section.

Done and acknowledged

p 5678, l 21-23: "Photochemical production and loss rates of ozone rely on the main gas-phase reactions driving the NO_x, HO_x, ClO_x, BrO_x catalytic cycles." I think it would be easier to understand, if this sentence would come before the previous one.

Done and acknowledged

p 5679 l 8: "In the present concentration-driven experiments..." -> "In the concentration-driven experiments presented here..."

Done and acknowledged

p 5679, 19-10: "...provided by CMIP5" -> according to the CMIP5 protocol

Done and acknowledged

p 5679, l 18: "3 non-vegetated surfaces" -> 3 non-vegetated surface types

Done and acknowledged

p 5680, l 22: "This is a key advantage of this approach as most the..." -> A key advantage of this approach is that most of the ... without any additional parameters needed.

Done and acknowledged

p 5681, l 26: "The biogeochemical model of CNRM-ESM1..." -> The ocean biogeochemical model... or similar

Done and acknowledged

p 5682, l 4: "Dependence of growth to..." -> Dependence of growth on

Done and acknowledged

p 5682, l 12: into -> in

Done and acknowledged

p 5682, l 18-19: either "following the formulation of Geider et al..." or remove "formulation".

Done and acknowledged

p 5683, l 12: What is "Princeton atmospheric forcing"? Please provide a reference here.

Done and acknowledged

p 5687, l 26: detailed in (Voltaire et al., 2013) -> detailed in Voltaire et al., 2013

Done and acknowledged

p 5688, l 8: acronym GPCP should be explained

Done and acknowledged

Section 4.2.3: CNRM-CM5.2 is used while CNRM-CM5.2 is used in figure caption. Please use consistent names.

Done and acknowledged

p 5694, l 6: "Figure 10 shows that the amplitude of annual mean GPP as..." Fig 10 shows the annual mean, I suggest deleting "the amplitude of".

Done and acknowledged

p 5694, l 9: "...patterns of high GPP (values)." Please add values or remove the "(values)"

Done and acknowledged

p 5694, l 18: "...Princeton university forcings (REF)..." Yes, please add a reference.

Done and acknowledged

p 5700, l 5: "... uptake of CO₂ of about 2.1 and 1.7 Pg C y⁻¹ for land and ocean..." Which year do these numbers correspond to? Is it 2005, or a mean over the last decade?

Done and acknowledged

Figure 6d: The scale could be narrower (perhaps -2 to 2 psu?), since larger biases seem to occur only at the surface and the surface bias is already depicted in 6b. As it is now it is difficult to see the structures of the salinity biases at depth.

Done and acknowledged

Figure 9a: In the figure legend it says PAR is given in the figure caption it says RSDS. Please check and correct.

Done and acknowledged

Figure 13: This figure is really difficult to read, since the different sizes of the symbols are difficult to distinguish. I think it would be much easier for the reader to have one panel per depth with all 4 tracers.

Done and acknowledged

Reviewer #2:

The article by S  f  rian et al. presents the first Earth-System Model developed at CNRM. It is based on the CNRM-CM5 coupled climate model (Voldoire et al. 2013) and includes the ISBA module for a representation of the land surfaces in the carbon cycle. The ocean biogeochemistry (PISCES) was already implemented in CNRM-CM5. The subject of the paper particularly fits within the scope of GMD. The overall structure of the paper and the quality of the science are very good, and the paper is well written. The main features of the physical behavior of the model are presented and evaluated. The protocol of the preparation of the model and the realization of the simulations (spin-up, pre-industrial control and historical simulation) are rigorously done. The amount of work and knowledge is impressive. Without a doubt, the authors are true experts in their fields.

[We appreciate the reviewer’s careful reading and suggestions for corrections. Most of his/her suggestions and comments are addressed in the revised manuscript.](#)

However, the interpretation of the evaluation results deserves revisions (specific comments below). The authors use words like “realistically”, “moderate” or “reasonably well-simulated” to describe the behavior of the model compared with observations. This is totally subjective and does not have its place in such a paper. I understand what the authors mean by this, and it would be acceptable in an oral presentation, but not in a scientific paper. These statements should be supported by more objective quantifications or comparisons with other models. For instance, how can we say that a model is “realistic”, or an agreement is “moderate”? Two different paths can be considered: either using statistics that objectively quantify the agreement (for instance, “my model explains XX% of the variance of the observations, and we assume that above [a meaningful threshold], the model meaningfully reproduces the observations on this diagnostic”), or by comparing the results with other models that will be used as benchmark. Both approaches are used in the paper (notably the comparison with CNRM-CM5) but not systematically. For instance, Figures 6, 7 and 8 of the supplementary materials are among the most interesting figures for they put the model in the multi-model intercomparison context. I strongly recommend taking advantage of the availability of the CMIP5 ESMs outputs to strengthen the evaluation of CNRM-ESM1 and see how it compares with other models. One way to do it is a portrait diagram showing synthetic metrics of model-data agreement (see Anav et al. 2013, Fig18) with the results of other ESMs for the carbon cycle variables. Nevertheless, this is only a possibility and the most important point to me is to remove, as much as possible, the subjectivity from the presentation of your results. In the specific comments I point out the issues that need more robust support.

One truly annoying point is the use of the supplementary materials. The authors do not specify which figure is pointed out by the reference to the supplementary materials, and the reader has to guess which figure he should look for. I still don’t

know if you use Figure 1 or not. Following this, I recommend the publication of the paper in GMD after major revisions.

We agree with the referee's comments and we have strengthened the model evaluation using quantitative evaluation in the revised manuscript.

Specific comments

Abstract: the end of the abstract is about the too strong flow of North Atlantic Deep Water and the accumulation of anthropogenic carbon in the deep ocean. Meanwhile, those points are not reported in the summary and conclusion section (section 5). I suggest either presenting these points more comprehensively in section 5 or removing them from the abstract (maybe focus on something else) so that the abstract and last section are aligned in terms of contents and highlights. As well, it is a shame to end the abstract the way it is right now, with a quite negative statement. A focus on the good performances of the model would be more appropriate.

We understand the referee point of view. However, to our point of view, it is fundamental to highlight model weaknesses in an evaluation paper and hence to point out future leads of improvements. We have thus chosen to include a small paragraph on the biases in anthropogenic carbon storage in the conclusion section.

Submitted:

“This change is attributed to improved water conservation in the ocean-sea ice model as well as a higher coupling frequency that induces a stronger northward flow of deep water masses from the Southern ocean. While the simulated anthropogenic carbon storage agrees with 1994 observation-based estimates, the ocean carbon sink falls within the lower range of the combination of observation and model estimates over the recent years (Le Quéré et al., 2014).”

Revised:

“This change is attributed to a stronger northward flow of deep water masses from the Southern ocean which improves the vertical distribution of biogeochemical tracers. However, the strengthening of the meridional flow of deep water masses has also distorted the vertical structure of some carbon-related fields. Indeed, the unrealistic flow of North Atlantic deep water of about 26.1 Sv tends to deplete the stock of anthropogenic carbon storage between surface and 1200 m (Figure 16c) and consequently to increase it at depth. Since biases in anthropogenic carbon storage compensate across the water column, the simulated anthropogenic carbon storage agrees with 1994 observation-based estimates. Regarding the ocean carbon sink, CNRM-ESM1 simulates a global ocean carbon sink that falls within the lower range of the combination of observation and model estimates over the recent years (Le Quéré et al., 2014).”

Page 5688, line 20: the expression ‘non-significant’ suggests that there is a statistical support behind this statement. Change it for something like ‘very

small' and add an estimate of this change in percentage (of the average field for example).

Please see the response below.

Page 5688, line 25: please specify which figure in the supplementary materials is targeted by this mention. I assume you mean Figure 2, but add it for the convenience of the reader. Additionally, I'm not convinced by this figure. Where am I supposed to see an improvement between CM5 and ESM1? Either I don't understand the meaning of the figure therefore I assume it is not correctly explained or there is no comparison with observations on this figure and I don't see how it should be able to show any improvement. Please clarify.

According to the comments of the both referees, we have changed the wording of this section for sake of clarity.

Submitted:

"The mismatch between simulated and GPCP observed PR over continents is slightly improved during the boreal winter with a bias reduced by $0.014 \text{ mm day}^{-1}$ in CNRM-ESM1. Summer PR is similar between the two models with non-significant changes in simulated values ($<10^{-5} \text{ mm day}^{-1}$) but their geographical patterns have been slightly degraded in CNRM-ESM1 compared to CNRM-CM5. Although weak, changes induced by the ISBA biophysical coupling slightly improve the representation of the seasonal cycle in PR over Northern mid-latitude continents by amplifying the seasonal maximum and shifting it from June in CNRM-CM5 to July in CNRM-ESM1 (supplementary materials)."

Revised:

"Although weak, changes induced by the ISBA biophysical coupling slightly affect the representation of the seasonal cycle in PR over the vegetated regions (Figure S1). These lead to improve the simulated PR in CNRM-ESM1 compared to CNRM-CM5 over some vegetated regions during the growing season (spring-summer). Between 30°N and 60°N , the averaged error in simulated PR compared to GPCP is reduced by 0.12 mm day^{-1} in CNRM-ESM1 compared to that of CNRM-CM5. Over the tropics (30°S - 30°N), simulated PR is also improved in CNRM-ESM1 compared to CNRM-CM5 but to a lesser extent with a reduction of the averaged error by 0.06 mm day^{-1} with respect to GPCP. Although PR have been improved over some region, their geographical patterns have been degraded in CNRM-ESM1 compared to CNRM-CM5, especially during the winter."

Page 5693, line 16; page 5694, line 12, Line 662, Lines 687-688: specify which figure in the supplementary materials is targeted by this mention for the reader's convenience.

We apologize for mistakes. Supplementary figures are now clearly mentioned in the revised manuscript.

Page 5689, lines 16-18: what I see on Figure 6ab is a bias map, i.e. a quantification of model errors. I have no particular mean to tell if those biases are sufficiently small to tell that the model “realistically simulates” the observed climate (same for “moderate” on line 18). I suggest either adding the results of CNRM-CM5 (either on this figure or another one) to put this statement in perspective of a model that can be used as a benchmark, or add an objective quantification of the model-data agreement that could make more sense than qualifications like ‘realistic’.

We agree with the referee. Yet, this section is essentially dedicated to the skill-assessment of CNRM-ESM1 ocean drivers. We include a basic metrics from CNRM-CM5 to strengthen and support our model-data assessment. The objective intercomparison of CNRM-ESM1 to previous model version is detailed 4.2.3. In agreement with referee comments, we have included new supplementary figures comparing model-data agreement for CNRM-ESM1 and CNRM-CM5 to support statistical metrics summarized in the Taylor diagram (Figure 9 in the submitted manuscript).

Page 5690, line 1-2: I don’t understand how you can say that the vertical structure of S matches better with WOA2013 than T. They don’t have the same units, and we have no idea about the uncertainty linked with the diagnostic to judge if the difference is smaller for S than T. Either provide objective elements to support your statement, or remove this sentence.

According to the referee’s comments, we have amended the section as follows.

Submitted:

“At depth, the vertical structures in T and S present moderate deviations from WOA2013 observations. T is underestimated by $\sim 2^{\circ}\text{C}$ within the first 1000 m of the Atlantic and Pacific oceans, except in the deep water formation zone (North Atlantic, North Pacific and Southern Ocean), where the model displays positive biases. Contrasting to T, the vertical structure of S matches well with WOA2013 observations. Deviations from the observed S profile are found in deep water formation zones where haline biases tend to compensate for the warm bias in T, enabling deep convection of water masses.”

Revised:

“At depth, the vertical structures in simulated T and S display biases from those estimated from WOA2013 observations. T is underestimated by $\sim 2^{\circ}\text{C}$ within the first 1000 m of the Atlantic and Pacific oceans, except in the deep water formation zone (North Atlantic, North Pacific and Southern Ocean), where the model displays positive biases. The largest deviation in vertical structure of simulated S from that estimated from WOA2013 are found in deep water formation zones where haline biases of about ~ 1 psu tend to compensate for the warm bias in T, enabling deep convection of water masses.”

Page 5691, lines 3-4: What are your criteria to say that the model ‘reproduces well’ the pattern of the observations? Replace ‘CNRM-ESM1 reproduces well the regional pattern of MLDmax’ with ‘CNRM-ESM1 simulates the main regional features of MLDmax’.

Done and acknowledged.

Page 5691, lines 19-20: This sentence is too vague. Either remove it, or put this result in perspective with another model (if so, we need to see the figure).

Right, we have amended the section as follows.

Submitted:

“Compared to the observation-derived estimates, the MLD_{min} is reasonably well simulated in CNRM-ESM1. Compared to the previous model versions (Séférian et al., 2013; Voldoire et al., 2013), CNRM-ESM1 fails at reproducing the deepest values of mixing in the Southern Ocean and the Tropics. These are tightly linked to the current parameterization of the ocean mixing employed in CNRM-ESM1 implying a contribution of the surface wind energy to the mixing below the MLD.”

Revised:

“Compared to the observation-derived estimates, CNRM-ESM1 captures the main regional pattern of MLD_{min} but the model fails at reproducing the deepest values of mixing in the Southern Ocean and the Tropics. This bias might be linked to the current parameterization of the ocean mixing employed in CNRM-ESM1 because previous model version using this parameterization also exhibited similar patterns of errors as detailed in (Séférian et al., 2013; Voldoire et al., 2013).”

Section 4-2-3: I have an issue with this section. You talk about skills that are ‘different’, or ‘similar’. But objectively, on your plot, you don’t have the means to say that two correlations are truly different (statistically speaking). It is even more the case when you compare the behavior of the correlations for two different variables, or two different seasons, since they are not computed on the same number of degrees of freedom. Your statement “the difference in simulated SSS between the two models can be attributed to [...]” is too strong compared with the true ability of those metrics to demonstrate what you say. In my opinion, metrics are mainly good tools to highlight outliers, but not so much to demonstrate any physical link (even if, sometimes, we can ‘understand’ their behavior). I would be much more convinced by a set of well-chosen maps of the biases of SSS, PR and sea ice, with both model versions (CM5 and ESM) side to side. They would show a much more reliable proof of the difference between the models and where does it come from. By the way, Figure 3c of the supplementary materials looks weird to me. On panel (a) mainly, there is sea ice in the Labrador Sea (between 0-10%). There is no sea ice in this region in panel (b), thus the difference should not be zero in panel (c) in the Labrador Sea. You might have an issue with the display of your results.

We thank the referee for his/her careful reading.

Indeed, correlation coefficients computed with at annual time scales have to be compared with each other, not with those computed at seasonal time scales. With that said, the referee is right a Taylor diagram has to be supported with maps of model-data errors. We have therefore included several supplementary Figures of model-data errors

for temperature, salinity and mixed-layer depth from both CNRM-ESM1 and CNRM-CM5.2 to support the Taylor diagram presented in the manuscript.

Then, in agreement with first reviewer comments, we have moved Figure S3 into the main text as Figure 10. This latter will help the reader to better understand the influence of the ocean-atmosphere coupling frequency on sea-ice modeling. This Figure has been updated and corrected in agreement with above-mentioned comments concerning Figure 8.

Page 5696, lines 10-21: What about removing the El-Nino years before the computation of your climatology of CNRM-ESM1 to try to match the methodology of Takahashi et al. (2010)? Either provide a justification for not doing it, or provide an additional figure with the El-Niño years removed.

In agreement with the comments and suggestions of the first referee, we have chosen to provide a comparison with another data product which includes El-Niño influence on sea-air carbon fluxes (Figure R1). Figure R1 is also provided in supplementary materials.

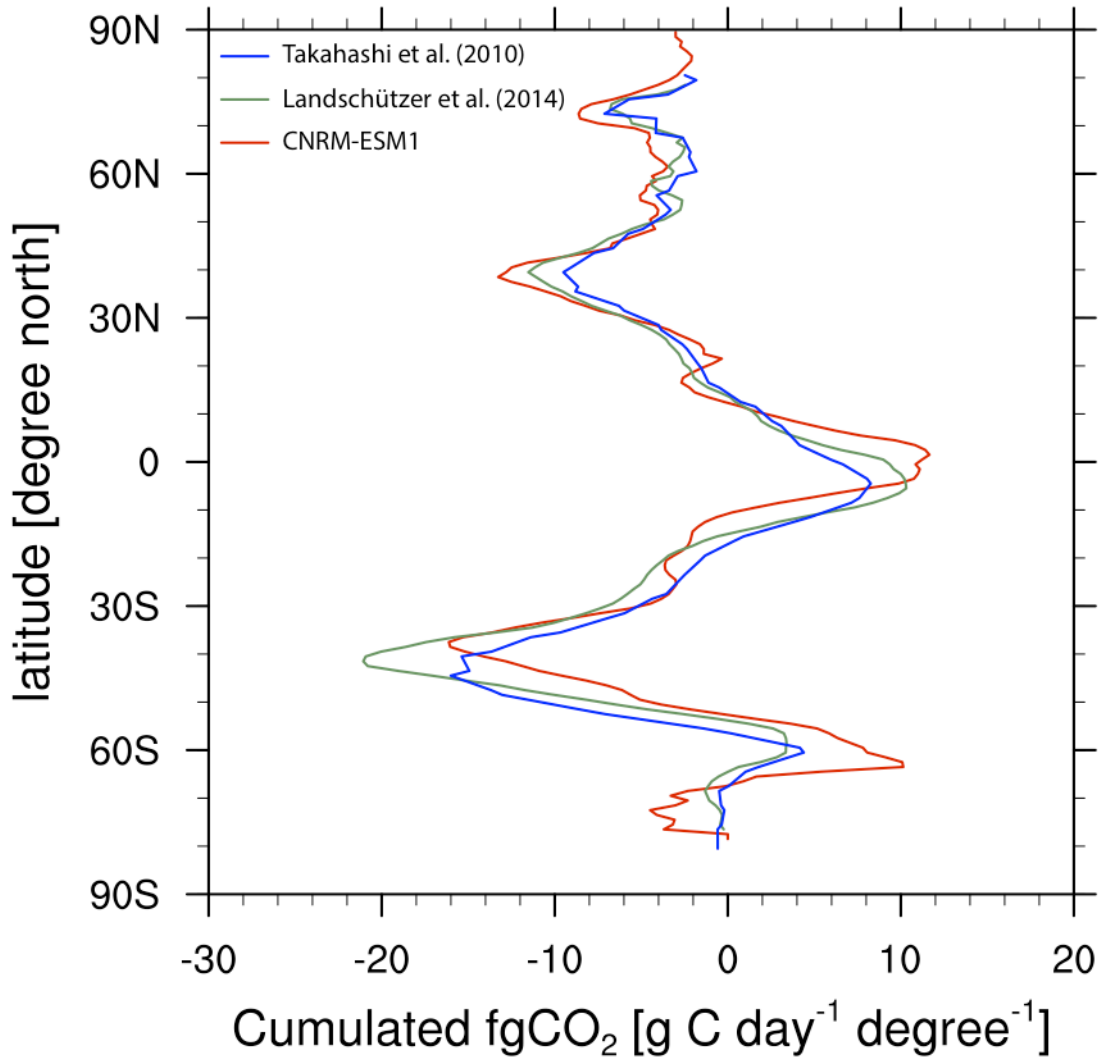


Figure R1: Zonally-cumulated ocean carbon fluxes (fgCO_2) averaged over 1986-2005 from observation-derived estimates and as simulated by CNRM-ESM1. Observation-derived estimates from Takahashi et al. (2010) and Landschützer et al. (2014) are represented with blue and green solid lines, respectively. Result from CNRM-ESM1 is given with a solid red line.

Minor points

Page 5673, line 6-7: suggest adding a reference to Flato (2011)

Done and acknowledged

Page 5693, line 8: looking at the Taylor Diagram, the standard-deviation ratio for MLD (on average) is around 0,5. Therefore, it shows that the model underestimates (rather than overestimates) the spatial variations of this field compared with the observation- derived MLD product of Sallée et al. 2010.

Done and acknowledged

Page 5690, line 5: suggest changing “Thanks to” with “Because of”

Done and acknowledged

Page 5690, line 27: define in this sentence what MLDmax and MLDmin are (for convenience), or explicitly refer to the caption of the figure.

Done and acknowledged

Figure 8: the color bar seems to be incoherent with the contour line for the model. If I'm correct, the dashed contour line highlights the isoline 15 but it remains within the 0-10 range of the color field. This is really a minor point but you might have a look at it to correct it.

We appreciate reviewer careful reading. There was indeed an error in the sea concentration labeling. This error is now corrected in the revised manuscript.

Page 5693, lines 5-6: add ‘apart from a tendency to show higher variability (standard- deviation ratio).

This point is especially true for the mixed-layer depth and was already mentioned in this subsection of the submitted manuscript.

Page 5694, line 11: replace “lesser extend” with “lower extent”

Done and acknowledged

Figures 10, 11, 12: the color palette with white in the middle should be used for differences (as on Figure 5), not for a full field. Change it for a meaningful color palette (i.e. in the same way as the color palette you use for sea ice cover). I would also suggest adding the difference maps for all those fields. These to avoid leaving the reader playing a game of ‘guess where it’s greener’.

We agree with the referee regarding the choice of the color palette. We have updated the Figures accordingly.

Regarding the general comments of the referee, we do not want to include too much materials in the manuscript since an objective skill-assessment of CNRM-ESM1 versus other IPCC-class Earth system model is now provided in the main text to support the discussion section.

Page 5694, line 18: it looks like the authors forgot to change (REF) with the right reference of the Princeton University Forcing

Done and acknowledged

Page 5695, line 10: replace “compared to” with “than”

Done and acknowledged

Page 5696, line 8: I’m not too sure about the expression “carbon cycling”. . . I suggest double-checking that it is truly correct.

This is a correct wording.

Page 5696, line 8: replace ‘In term of’ with ‘In terms of’

Done and acknowledged

Page 5698, lines 24-26: need for a reference to support what you say about the origin of the biases in the equatorial upwelling systems.

This point is discussed in Landshutzer et al. (2014) which is already mentioned in this section. To support our statement, we have included comparison to Landshutzer et al. data product for sea-air CO2 fluxes as supplementary figure.

Page 5699, line 19: replace “following” with “after” to avoid repetition

Done and acknowledged

Page 5701, line 24: replace “discrepancies similar to” with “similar performances as” (more positive)

Done and acknowledged

References:

Le Quéré, C., Moriarty, R., Andrew, R. M., Peters, G. P., Ciais, P., Friedlingstein, P., Jones, S. D., Sitch, S., Tans, P., Arneeth, A., Boden, T. A., Bopp, L., Bozec, Y., Canadell, J. G., Chevallier, F., Cosca, C. E., Harris, I., Hoppema, M., Houghton, R. A., House, J. I., Jain, A., Johannessen, T., Kato, E., Keeling, R. F., Kitidis, V., Klein Goldewijk, K., Koven, C., Landa, C. S., Landschützer, P., Lenton, A., Lima, I. D., Marland, G., Mathis, J. T., Metzl, N., Nojiri, Y., Olsen, A., Ono, T., Peters, W., Pfeil, B., Poulter, B., Raupach, M. R., Regnier, P., Rödenbeck, C., Saito, S., Salisbury, J. E., SCHUSTER, U., Schwinger, J., Séférian, R., Segschneider, J., Steinhoff, T., Stocker, B. D., Sutton, A. J., Takahashi, T., Tilbrook, B., van der Werf, G. R., Viovy, N., Wang, Y. P., Wanninkhof, R., Wiltshire, A. and Zeng, N.: Global carbon budget 2014, *ESSDD*, 7(2), 521–610, 2014.

Lipschultz, F., Wofsy, S. C., Ward, B. B., Codispoti, L. A., Friedrich, G. and Elkins, J. W.: Bacterial transformations of inorganic nitrogen in the oxygen-deficient waters of the Eastern Tropical South Pacific Ocean, *Deep-Sea Res*, 37(10), 1513–1541, doi:doi:10.1016/0198-0149(90)90060-9, 1990.

Middelburg, J., Soetaert, K., Herman, P. and Heip, C.: Denitrification in marine sediments: A model study, *Global Biogeochem. Cycles*, 10(4), 661–673, 1996.

Orsi, A., Johnson, G. and Bullister, J.: Circulation, mixing, and production of Antarctic Bottom Water, *Progress in Oceanography*, 1999.

Séférian, R., Bopp, L., Gehlen, M., Orr, J., Ethé, C., Cadule, P., Aumont, O., Salas y Mélia, D., Voltaire, A. and Madec, G.: Skill assessment of three earth system models with common marine biogeochemistry, *Climate Dynamics*, 40(9-10), 2549–2573, doi:10.1007/s00382-012-1362-8, 2013.

Soetaert, K., Middelburg, J., Herman, P. and Buis, K.: On the coupling of benthic and pelagic biogeochemical models, *Earth-Sci Rev*, 51, 173–201, 2000.

Takahashi, T., Broecker, W. and Langer, S.: Redfield Ratio Based on Chemical-Data From Isopycnal Surfaces, *Journal of Geophysical Research-Oceans*, 90, 6907–6924, 1985.

Valcke, S.: The OASIS3 coupler: a European climate modelling community software, *Geoscientific Model Development*, 6(2), 373–388, doi:10.5194/gmd-6-373-2013, 2013.

Voltaire, A., Sanchez-Gomez, E., Salas y Mélia, D., Decharme, B., Cassou, C., Sénési, S., Valcke, S., Beau, I., Alias, A., Chevallier, M., Déqué, M., Deshayes, J., Douville, H., Fernandez, E., Madec, G., Maisonnave, E., Moine, M. P., Planton, S., Saint-Martin, D., Szopa, S., Tyteca, S., Alkama, R., Belamari, S., Braun, A., Coquart, L. and Chauvin, F.: The CNRM-CM5.1 global climate model: description and basic evaluation, *Climate Dynamics*, 40(9-10), 2091–2121, doi:10.1007/s00382-011-1259-y, 2013.

1 Development and evaluation of CNRM Earth-System model

2 – CNRM-ESM1

3 R. Sférian¹, C. Delire¹, B. Decharme¹, A. Voldoire¹, D. Salas y Melia¹, M.
4 Chevallier¹, D. Saint-Martin¹, O. Aumont², J.-C. Calvet¹, D. Carrer¹, H. Douville¹, L.
5 Franchistéguy¹, E. Joetzer³, S. Sénési¹

6 ¹ CNRM-GAME, Centre National de Recherches Météorologiques-Groupe d'Etude
7 de l'Atmosphère Météorologique, Météo-France/CNRS, 42 Avenue Gaspard Coriolis,
8 31057 Toulouse, France

9 ² Sorbonne Universités (UPMC, Univ Paris 06)-CNRS-IRD-MNHN, LOCEAN-IPSL
10 Laboratory, 4 Place Jussieu, F-75005 Paris, France

11 ³ Montana State University, Institute on Ecosystems, Department of Ecology, 111
12 AJM Johnson Hall, Bozeman, Montana 59717, USA

13 Abstract:

14 We document the first version of the Centre National de Recherches Météorologiques
15 Earth system model (CNRM-ESM1). This model is based on the physical core of the
16 CNRM-CM5 model and employs the Interactions between Soil, Biosphere and
17 Atmosphere (ISBA), and the Pelagic Interaction Scheme for Carbon and Ecosystem
18 Studies (PISCES) as terrestrial and oceanic components of the global carbon cycle.
19 We describe a preindustrial and 20th century climate simulation following the CMIP5
20 protocol. We detail how the various carbon reservoirs were initialized and analyze the
21 behavior of the carbon cycle and its prominent physical drivers. Over the 1986-2005
22 period, CNRM-ESM1 reproduces satisfactorily several aspects of the modern carbon
23 cycle. On land, the model captures the carbon cycling through vegetation and soil,
24 resulting in a net terrestrial carbon sink of 2.2 Pg C y⁻¹. In the ocean, the large-scale
25 distribution of hydrodynamical and biogeochemical tracers agrees with a modern
26 climatology from the World Ocean Atlas. The combination of biological and physical
27 processes induces a net CO₂ uptake of 1.7 Pg C y⁻¹ that falls within the range of recent

roland seferian 23/10/15 17:00

Deleted: introduce and

roland seferian 23/10/15 17:02

Deleted: module

roland seferian 23/10/15 16:59

Deleted: reasonably

roland seferian 23/10/15 17:03

Deleted: well

28 estimates. Our analysis shows that the atmospheric climate of CNRM-ESM1
29 compares well with that of CNRM-CM5. Biases in precipitation and shortwave
30 radiation over the Tropics generate errors in gross primary productivity and ecosystem
31 respiration. Compared to CNRM-CM5, the revised ocean-sea ice coupling has
32 modified the sea-ice cover and ocean ventilation, unrealistically strengthening the
33 flow of North Atlantic deep water (26.1 ± 2 Sv). It results in an accumulation of
34 anthropogenic carbon in the deep ocean.

35

36

37 **1. Introduction**

38 Earth system models (ESMs) are now recognized as the current state-of-the-art
39 models (IPCC, 2013), expanding the numerical representation of the climate system
40 of the 4th Assessment Report (IPCC, 2007). They enable the representation of subtle
41 non-linear interactions and feedbacks of different magnitude and signs of various
42 biogeochemical and biophysical processes with the climate system. The latter
43 contribute, in addition to the atmospheric radiative properties and global climate
44 dynamics, to determine the Earth's climate variability (Arora et al., 2013; Cox et al.,
45 2000; Friedlingstein and Prentice, 2010; Schwinger et al., 2014; Wetzel et al., 2006).

46 Although there is no uniformly accepted definition, ESMs generally bring together a
47 global physical climate model and land and ocean biogeochemical modules
48 (Bretherton, 1985; Flato, 2011). As such, they enable the representation of the global
49 carbon cycle. The models of this class have played a larger role in the 5th IPCC report
50 than in previous reports, primarily through their contribution to the concentration- and
51 emission-driven experiments that compose CMIP5.

52 Even if the concept of Earth system modeling is being extended to include further
53 processes and reservoirs (e.g., nitrogen cycle, aerosols) (Hajima et al., 2014), there are
54 still large uncertainties in the representation of the carbon cycle and its interactions
55 with climate (Anav et al., 2013a; Friedlingstein et al., 2013; Piao et al., 2013). To
56 reduce them, there is a need for improvements of both physical and ecophysiological

57 parameterizations (Dalmonech et al., 2014), and for the development of observation-
58 based methods to constrain model projections (Wenzel et al., 2014). But the reduction
59 of carbon cycle-climate uncertainties also requires a greater number and diversity of
60 ESMs. This path is promoted and followed by various international initiatives like the
61 Global Carbon Budget (<http://www.globalcarbonproject.org/>) that sequentially
62 incorporate more and more models into their analyses (Le Quéré et al., 2013; 2015).

roland seferian 23/10/15 17:16

Deleted: ensemble

63 This manuscript documents the first IPCC-class ESM developed at Centre National de
64 Recherches Météorologiques and provides a basic evaluation of the model's skill.
65 This model is based on the CNRM-CM5.1 climate model jointly developed by
66 CNRM and Cerfacs (Centre Européen de Recherche et de Formation Avancée en
67 Calcul Scientifique), which has contributed to the fifth phase of the Coupled Model
68 Inter- comparison Project (CMIP5) (Voldoire et al., 2013). CNRM-CM5.1 did not
69 include a representation of the global carbon cycle but accounted for chemical-climate
70 interactions with an interactive stratospheric chemistry module (Cariolle and
71 Teyssedre, 2007). While this configuration of CNRM-CM5 contributed to the CMIP5
72 results publicly released, a first intermediate version of the CNRM ESM was
73 developed with the inclusion of the marine biogeochemistry model PISCES (Aumont
74 and Bopp, 2006). This model version was evaluated against modern oceanic
75 observations (Séférian et al., 2013) and employed in various studies (Frölicher et al.,
76 2014; Laufkötter et al., 2015; Schwinger et al., 2014; Séférian et al., 2014).

77 A terrestrial carbon cycle module is being developed at CNRM since the 2000s
78 (Calvet and Soussana, 2001; Calvet et al., 2008; 2004; Gibelin et al., 2008; 2006), but
79 it has never been coupled to an atmosphere-ocean model. This carbon cycle module
80 evolved from the physically-based ISBA model (Noilhan and Mahfouf, 1996; Noilhan
81 and Planton, 1989) and is able to simulate the surface carbon fluxes and the terrestrial
82 carbon pools. The carbon fluxes module was extensively tested over France and
83 Europe (Sarrat et al., 2007; Szczypta et al., 2012), and the carbon cycle module was
84 tested for temperate and high latitude regions (Gibelin et al., 2006; 2008) and was
85 used more recently in studies of carbon cycling over the Amazon basin (Joetzjer et al.,
86 2015; 2014), permafrost regions (Rawlins et al., 2015) and at global scale (Carrer et
87 al., 2013b). In this work, this terrestrial carbon cycle module is coupled to a global
88 climate model for the first time.

89 Here, we present a first evaluation of the CNRM-ESM1. In section 2, we describe the
90 model, focusing on the Earth system's components and aspects of the climate model
91 that are particularly relevant to the global carbon cycle. We describe in section 3 the
92 pre-industrial control and 20th century experiments that we conducted, together with
93 the forcings used and how the experiments were initialized. In section 4, we present
94 and discuss the results of these experiments. We summarize the results in section 5
95 and present conclusions.

96

97 2- CNRM-ESM components

98 2-1 The physical core

99 CNRM-ESM1 is based on the physical core of the CNRM-CM5.1 Atmosphere-Ocean
100 General Circulation Model, extensively described in Voltaire et al. (2013), which
101 accounts for the physical and dynamical interactions occurring between atmosphere,
102 land, ocean and sea-ice.

roland seferian 23/10/15 18:31

Deleted: OGCM model

roland seferian 23/10/15 19:36

Deleted: (ARPEGE-Climat, SURFEX, NEMO, GELATO, respectively)

103 The atmospheric component is based on version 6.1 of the global spectral model
104 ARPEGE-Climat which corresponds to an updated version of the atmospheric code
105 used in CNRM-CM5.1. This updated version of the atmospheric code derives from
106 cycle 37 of the ARPEGE-IFS (Integrated Forecast System) numerical weather
107 prediction model developed jointly by Météo-France and the European Center for
108 Medium-range Weather Forecast. In CNRM-ESM1, the geometry, parameterizations
109 and dynamics have been chosen to match the choices made for CNRM-CM5.1. Thus
110 differences are mainly due to debugging and recoding. The atmospheric physics and
111 dynamics are solved on a T127 triangular truncation that offers a spatial resolution of
112 about 1.4° in both longitude and latitude. Consistently to CNRM-CM5.1, CNRM-
113 ESM1 employs a ‘‘low-top’’ configuration with 31 vertical levels that extend from
114 the surface to 10 hPa in the stratosphere. The layers are unevenly distributed with 6
115 layers below 850 hPa except in regions of high orography, nine layers above 200 hPa
116 and four layers above 100 hPa. The dynamical core of the model, the radiative scheme
117 for longwave and shortwave as well as the physical parameterization for deep and
118 shallow convection are identical to those employed in CNRM-CM5.1. The reader is

roland seferian 23/10/15 19:38

Deleted: whereas

roland seferian 23/10/15 19:38

Deleted: was based on version 5.2

119 referred to Voltaire et al. (2013) for the original description of the atmospheric model
120 parameterizations.

121 The land-surface component is an updated version of the SURFface EXternalisée
122 modeling platform (SURFEXv7.3) (Masson et al., 2013b) associated with the Total
123 Runoff Integrating Pathways (TRIP) river routing model (Oki and Sud, 1997).
124 SURFEX was designed so that the same code could be run offline or coupled to a
125 GCM, to allow easy transfer from offline improvements to the coupled model and to
126 be able to compare online and offline runs.

127 This model prognostically computes the exchange of energy, water and carbon
128 between the atmosphere and three types of natural surfaces: Land, free water bodies,
129 oceans or seas. The energy, water and carbon balances are calculated separately for
130 each surface type and area-averaged over each atmospheric grid cell. The natural land
131 surfaces are represented by the module originally developed by Noilhan and Planton
132 (1989). This module solves the surface energy and soil water budgets using the force-
133 restore method and a composite soil-vegetation-snow approach. The version used here
134 is the same as for CNRM-CM5.1; e.g. the soil hydrology uses 3 vertical layers (Boone
135 et al., 1999) while soil temperature is solved using 4 vertical layers. In CNRM-ESM1,
136 land surface albedo benefits from an improved spatial representation derived from
137 MODIS satellite measurements (Carrer et al., 2013a) except for the area covered by
138 snow for which the albedo is prognostically computed following Douville et al.
139 (1995). Over water bodies and oceans, we use the CNRM-CM5.1 parameterization for
140 momentum and energy fluxes except for the sea-to-air turbulent fluxes that are
141 computed from the COARE scheme (Fairall et al., 2003). Interactions between the
142 land surface energy and water budgets and the terrestrial carbon cycle module are
143 detailed in section 2.3.1.

144 The ocean component uses version 3.2 of the NEMO model (Madec, 2008) in the
145 ORCA1L42 configuration. This configuration offers a horizontal resolution from 1°
146 to 1/3° near the equator and 42 levels in depth. The vertical discretization uses a
147 partial-step formulation (Barnier et al., 2006), which ensures a better representation of
148 bottom bathymetry and thus stream flow and friction at the bottom of the ocean.
149 Ocean dynamics and physics is solved using a timestep of 1 hour. Vertical physics

roland seferian 1/12/15 12:05

Deleted: The main difference from the CNRM-CM5.1 atmospheric model is the improved treatment of volcanic aerosols.

150 relies on the parameterization chosen for the CNRM-CM5.1 climate model. The
151 mixed layer dynamics is parameterized using a double diffusion process (Merryfield
152 et al., 1999), Langmuir cell (Axell, 2002) and account for the contribution of surface
153 wave breaking (Mellor and Blumberg, 2004). A parameterization of bottom
154 intensified tidal-driven mixing similar to Simmons et al. (2004) is used in
155 combination with a specific tidal mixing parameterization in the Indonesian area
156 (Koch-Larrouy et al., 2010; 2007). Finally, CNRM-ESM1 benefits from an improved
157 Turbulent Kinetic Energy (TKE) closure scheme (Madec, 2008), based on the Blanke
158 and Delecluse (1993) TKE. This parameterization allows a fraction of surface wind
159 energy to penetrate below the base of the mixed layer ensuring a better coupling
160 between surface wind and subsurface mixing. The main difference from the CNRM-
161 CM5.1 ocean model is the explicit modulation of the radiative shortwave penetration
162 into the ocean by marine biota (Lengaigne et al., 2009; Mignot et al., 2013), which is
163 further detailed in section 2.3.2.

164 | The sea-ice model used in CNRM-ESM1 is GELATO6. This model employs the
165 same horizontal grid as NEMO and solves sea-ice dynamics and thermodynamics
166 every 6 hours. This model represents an updated version of the former sea-ice model
167 used in CNRM-CM5.1 (Voldoire et al., 2013). In GELATO6, sea-ice dynamics is
168 computed using the Elastic-Viscous-Plastic scheme proposed by Hunke and
169 Dukowicz (1997) formulated on an Arakawa C-grid (Bouillon et al., 2009). To
170 simulate the response of sea ice to convergence-divergence movements, GELATO6
171 employs a redistribution scheme derived from Thorndike et al. (1975). This scheme
172 ensures the representation of the rafting phenomenon for the slab of sea ice thinner
173 than 0.25 m and of ridging for the slab thicker than 0.25 m. GELATO6 includes a
174 thermodynamic scheme that resolves the evolution of four ice thickness categories (0–
175 0.3, 0.3–0.8, 0.8–3 and over 3 m). These four slabs of sea ice are modeled with 10
176 vertical layers unevenly distributed across the slab thickness. An enhanced resolution
177 at the top of the slab is used to better represent the evolution of sea ice in response to
178 the high frequency variability of the atmospheric thermal forcing. Besides, all sea-ice
179 slabs may be covered with one snow layer. In GELATO6, the snow layer is
180 considered to occult the transfer of light across the snow-sea ice-ocean continuum.

181 | This snow layer can age or form ice using the formulation described in Salas y Mélia
182 (2002). Since CNRM-CM5.1, the coupling between NEMO and GELATO has been

roland seferian 10/12/15 19:46

Formatted: Space Before: 0 pt, After: 0 pt, No widow/orphan control, Don't adjust space between Latin and Asian text, Don't adjust space between Asian text and numbers, Tabs: 0,99 cm, Left + 1,98 cm, Left + 2,96 cm, Left + 3,95 cm, Left + 4,94 cm, Left + 5,93 cm, Left + 6,91 cm, Left + 7,9 cm, Left + 8,89 cm, Left + 9,88 cm, Left + 10,86 cm, Left + 11,85 cm, Left

roland seferian 2/12/15 14:22

Formatted: English (US)

roland seferian 2/12/15 14:22

Formatted: Font:12 pt, Font color: Auto, English (US)

183 revised in order to improve the conservation of water and salt. In the previous model
184 version, CNRM-CM5.1, there was a large drift in salinity (-0.011psu/century) and in
185 sea level (-21 cm/century). These were caused by (1) the melting of land glaciers
186 (other than Antarctic and Greenland) that was not routed to the ocean and (2) an
187 erroneous coupling between sea-ice and ocean models. The coupling did not take into
188 account the fact that sea ice is levitating over the ocean in this version of NEMO.
189 Although not severe, it resulted in a loss of water in the model. These errors have
190 been fixed in CNRM-CM5-2 and CNRM-ESM1 and hence reducing the residual
191 drifts in salinity to +0.001psu/century and in sea level to +1.2cm/century.

192 In CNRM-ESM1, exchanges of momentum, water and energy between the
193 atmosphere and the surface models occurs every atmospheric timestep (i.e., 30
194 minutes) because SURFEX is a submodel of the atmospheric code. The coupling
195 between the atmosphere and the ocean models is handled by the OASIS coupler
196 (Valcke, 2013) and occurs every 6 hours. In CNRM-ESM1, the frequency of coupling
197 between the ocean and atmosphere models has been increased compared to CNRM-
198 CM5 in order to better resolve the dynamics of the sea-ice, which is resolved at this
199 timestep (i.e., 6 hours).

200

201 2-2 Atmospheric chemistry

202 The atmospheric chemistry scheme in CNRM-ESM1 consists of an interactive linear
203 ozone chemistry model MOBIDIC (Cariolle and Teyssedre, 2007) including a
204 representation of the three-dimensional atmospheric CO₂ mixing ratio.

205 As in CNRM-CM5, the ozone mixing ratio is treated as a prognostic variable with
206 photochemical production and loss rates climatology computed by a full chemistry
207 scheme. That is, the net photochemical production in the ozone continuity equation is
208 solved using a first-order Taylor series around the local value of the ozone mixing
209 ratio, air temperature, and the overhead ozone column. Ozone destruction terms are
210 used to parameterize the heterogeneous chemistry as a function of the equivalent
211 chlorine content prescribed for the actual year. All Taylor coefficients of this
212 linearized scheme were determined using a two-dimensional chemistry scheme with

roland seferian 2/12/15 14:22

Formatted: Font:12 pt, Font color: Auto, English (US)

roland seferian 2/12/15 14:22

Formatted: Font:12 pt, Font color: Auto, English (US)

roland seferian 2/12/15 14:22

Formatted: Font:12 pt, Font color: Auto, English (US)

roland seferian 2/12/15 14:22

Formatted: Font:12 pt, Font color: Auto, English (US)

roland seferian 2/12/15 14:22

Formatted: Font:12 pt, Font color: Auto, English (US)

roland seferian 2/12/15 14:22

Formatted: Font:12 pt, Font color: Auto, English (US)

roland seferian 2/12/15 14:22

Formatted: Font:12 pt, Font color: Auto, English (US)

roland seferian 2/12/15 14:22

Formatted: Font:12 pt, Font color: Auto, English (US)

roland seferian 2/12/15 14:21

Deleted: Since CNRM-CM5.1, the coupling between NEMO and GELATO has been revised in order to improve the conservation of water and salt.

roland seferian 27/11/15 16:39

Formatted: Highlight

roland seferian 2/12/15 14:21

Formatted: Font:14 pt, Font color: Red, French

roland seferian 23/10/15 19:50

Deleted: The coupling between

roland seferian 23/10/15 19:45

Deleted: is implicit and

roland seferian 23/10/15 19:45

Deleted: while

roland seferian 23/10/15 19:47

Deleted: t

213 56 constituents, 175 chemical reactions, and 51 photoreactions (Cariolle and Brard,
214 1985). [Photochemical production and loss rates of ozone rely on the main gas-phase](#)
215 [reactions driving the NO_x, HO_x, ClO_x, BrO_x catalytic cycles](#). In this version, the
216 gas-phase chemical rates were upgraded according to the recommendations of Sander
217 et al. (2006). While the ozone mixing ratio is fully described across the atmospheric
218 column, the linear ozone scheme was especially designed to resolve its evolution in
219 the stratosphere for the sake of radiative transfer calculation. Therefore, some
220 tropospheric chemical reactions are not taken into account in this scheme. The reader
221 is referred to a manuscript by Eyring et al. (2013) for an extensive evaluation of the
222 linear scheme versus TOMS satellite measurements and intercomparison with other
223 CMIP5 models.

roland seferian 23/10/15 19:53

Deleted: the JPL-2003-25 report

roland seferian 23/10/15 19:53

Deleted: (

roland seferian 23/10/15 19:53

Deleted: ,

roland seferian 23/10/15 19:54

Deleted: Photochemical production and loss rates of ozone rely on the main gas-phase reactions driving the NO_x, HO_x, ClO_x, BrO_x catalytic cycles.

224 In CNRM-ESM1, the atmospheric CO₂ mixing ratio can be treated as a prognostic
225 tracer. It responds interactively to natural CO₂ exchange from land and ocean every 30
226 min and 6 h, respectively, while anthropogenic carbon emissions are prescribed in this
227 model version. The CO₂ mixing ratio can affect the physical climate by impacting the
228 atmospheric radiative transfer computations and both terrestrial and marine carbon
229 uptake. In the concentration-driven experiments [presented here](#), the CO₂ mixing ratio
230 is however prescribed to the global yearly average atmospheric concentrations
231 [according to the CMIP5 protocol](#).

roland seferian 23/10/15 19:54

Deleted: present

roland seferian 23/10/15 19:55

Deleted: provided by

232

233 2-3 The biogeochemical components

234 2-3-1 Land biogeochemical model

235 In CNRM-ESM1, the interactions between climate and vegetation are handled by the
236 ISBA scheme embedded in the SURFEX surface model. The land biogeochemical
237 module in ISBA represents land surface physics, plant physiology, carbon allocation
238 and turnover, and carbon cycling through litter and soil (Calvet and Soussana, 2001;
239 Calvet et al., 1998; Gibelin et al., 2006; 2008). The land cover is represented by 9
240 plant functional types (PFT, given in Figure 1) and 3 non-vegetated surface [types](#) that
241 are determined spatially by the ECOCLIMAP physiographic database (Masson et al.,
242 2013a).

roland seferian 23/10/15 19:56

Deleted: s

243 ISBA uses a semi-mechanistic treatment of canopy photosynthesis and mesophyll
244 conductance following the Jacobs et al. (1996) and Goudriaan et al. (1985)
245 photosynthesis model. Mesophyll conductance in this framework corresponds to the
246 rate of photosynthesis under light-saturated conditions (Jacobs et al., 1996). As such,
247 this scheme does not explicitly account for Michealis-Menten kinetics of the Rubisco
248 enzyme found in Farquhar et al. (1980) and Collatz et al. (1992) models. ISBA
249 includes a representation of the soil water stress. Key parameters of the
250 photosynthesis model respond to the soil water stress, permitting the representation of
251 drought-avoiding and drought-tolerant responses to drought. For low vegetation and
252 for trees, the response to drought is based on the meta-analyses of Calvet (2000) and
253 Calvet et al. (2004) respectively.

254 The model simulates a ratio of intercellular CO₂ to atmospheric CO₂ that depends on
255 leaf-to-air saturation deficit, leaf temperature, and soil moisture. Assimilation is
256 calculated from this ratio, air CO₂ concentration, leaf temperature, and solar radiation
257 considering plant photosynthetic pathways: C₃ or C₄ (Calvet et al., 1998; Gibelin et al.,
258 2006). Stomatal conductance, which represents the vegetation control on gas transfer
259 (here, CO₂ and water vapor) between the leaves and the atmosphere, is finally
260 deduced from the assimilation rate. Leaf dark respiration is taken as a fraction of
261 maximum CO₂ limited rate of assimilation. Standard Q₁₀ response functions determine
262 the temperature dependencies of mesophyll conductance, CO₂ compensation point,
263 maximum photosynthetic rate and hence photosynthesis and respiration.

264
265 ISBA simulates the evolution of 6 reservoirs of biomass including leaf, wood, and
266 roots, and assumes the existence of metabolic/structural reservoirs of biomass
267 (Gibelin et al., 2008). Vegetation biomass is simulated interactively based on the
268 carbon assimilated by photosynthesis, and decreased by turnover and respiration. The
269 autotrophic respiration combines the respiration from all these reservoirs except the
270 woody reservoir that is supposed not to respire (Gibelin et al., 2008). In this model,
271 the vegetation phenology results directly from the carbon balance of the leaves.
272 Therefore, phenology is completely driven by photosynthesis and no growing degree-
273 day model is used. A key advantage of this approach is that most of the soil and
274 atmospheric drivers (the abiotic drivers) of phenology are accounted for without any
275 additional parameters (Szczypta et al., 2014). Leaf area index (LAI) is determined

roland seferian 1/12/15 12:41
Formatted: Space Before: 0 pt, After: 0 pt
roland seferian 1/12/15 12:41
Formatted: Justified

roland seferian 23/10/15 19:56
Deleted: This is a
roland seferian 23/10/15 19:57
Deleted: as
roland seferian 23/10/15 19:58
Deleted: .

276 from the leaf biomass and the specific leaf area index, which varies as a function of
277 leaf nitrogen concentration and plant functional type (Gibelin et al., 2006). ISBA uses
278 an implicit nitrogen limitation parameterization which is based on the meta-analysis
279 of leaf nitrogen measurement under CO₂ enrichment condition (Yin et al., 2002). This
280 simple implicit nitrogen limitation is based on the nitrogen dilution hypothesis, which
281 assumes that internal nitrogen content of a plant decrease under rising CO₂ due to the
282 accumulation of non-structural carbohydrates. It results that nitrogen dilution occurs
283 as soon as the increase in total biomass of a plant under rising CO₂ relative to growth
284 under ambient CO₂ is greater than the corresponding increase in total nitrogen. In
285 current version of ISBA, a linear decrease between specific leaf area index and
286 nitrogen to carbon ratio in leaves is used to mimic this mechanism (Calvet et al.,
287 2008), and hence to limit the net assimilation of atmospheric CO₂.

288
289 The soil organic matter and litter module in ISBA follows the soil carbon part of the
290 CENTURY model (Parton et al., 1988). Four pools of litter are represented. They are
291 differentiated by their location above- or below-ground and their content of lignin.
292 The litter pools are supplied by the fluxes of dead biomass from each biomass
293 reservoir (turnover) as described in Gibelin et al. (2008). The 3 soil organic matter
294 reservoirs (active, slow and passive) are characterized by their resistance to
295 decomposition with turnover times spanning from a few months for the active pool to
296 240 years for the passive pool. Heterotrophic respiration and hence the flux of CO₂
297 released to the atmosphere is the sum of respiration from the litter and soil organic
298 matter reservoirs. The rate of decomposition of organic matter is determined
299 essentially by soil moisture and temperature using a Q₁₀ dependence following the
300 formulation of Krinner et al. (2005). The rate of decomposition (by respiration)
301 depends also on the lignin fraction and the soil texture following Parton et al. (1988).

302 Changes in the carbon balance of the vegetation affect the energy and water balance,
303 and hence the climate, through changes in stomatal conductance and LAI. Through its
304 control on leaf transpiration, stomatal conductance affects latent heat flux and the
305 surface energy balance. LAI on the other hand affects evapotranspiration because it is
306 used to scale leaf-level to canopy level transpiration and evaporation from the
307 interception reservoir (water intercepted by leaves).

roland seferian 26/2/16 16:46
Deleted: ratio

roland seferian 1/12/15 12:38
Formatted: English (US)

roland seferian 22/2/16 12:14
Deleted: A

roland seferian 22/2/16 12:14
Deleted: model is implemented in ISBA growth model (Calvet et al., 2008)

roland seferian 1/12/15 12:38
Formatted: English (US)

roland seferian 22/2/16 12:19
Formatted: Subscript

roland seferian 1/12/15 12:38
Formatted: Subscript

roland seferian 1/12/15 12:38
Formatted: English (US)

roland seferian 1/12/15 12:38
Formatted: English (US), Subscript

roland seferian 1/12/15 12:38
Formatted: English (US)

roland seferian 1/12/15 12:38
Formatted: English (US), Subscript

roland seferian 1/12/15 12:38
Formatted: English (US)

roland seferian 1/12/15 12:38
Formatted: English (US)

roland seferian 1/12/15 12:37
Deleted: used to relate internal concentration of nitrogen to biomass and to

roland seferian 1/12/15 12:38
Formatted: English (US)

roland seferian 1/12/15 12:37
Formatted: Left, Space Before: 0 pt, After: 0 pt, No widow/orphan control, Don't adjust space between Latin and Asian text, Don't adjust space between Asian text and numbers, Tabs: 0,99 cm, Left + 1,98 cm, Left + 2,96 cm, Left + 3,95 cm, Left + 4,94 cm, Left + 5,93 cm, Left + 6,91 cm, Left + 7,9 cm, Left + 8,89 cm, Left + 9,88 cm, Left + 10,86 cm, Left + 11,85 cm, Left

roland seferian 1/12/15 12:37
Formatted: Space Before: 0 pt, After: 0 pt

308 In CNRM-ESM1, except for crops, changes in LAI don't affect the albedo of the
309 land-surface, as it is the case in some other models. As mentioned earlier, albedo is
310 derived from satellite observations corrected in the presence of snow, but does not
311 depend on the changes in LAI calculated by the model. This limits the biophysical
312 feedback from vegetation change to the atmosphere.

313

314 2-3-2 Ocean biogeochemical model

315 | The ocean biogeochemical model of CNRM-ESM1 is PISCES (Aumont and Bopp,
316 2006). This model simulates the biogeochemical cycles of oxygen, carbon and the
317 main nutrients with 24 state variables. Macronutrients (i.e., nitrate and ammonium,
318 phosphate, silicate) and micronutrient (i.e., iron) ensure a better representation of the
319 phytoplankton dynamics, because these 5 nutrients contribute to the nutrient limitation
320 process (Aumont et al., 2003). PISCES represents two size-classes of phytoplankton
321 | (i.e., nanophytoplankton and diatoms) Dependence of growth on temperature is
322 parameterized according to Eppley et al. (1969). Growth rate is also limited by the
323 external availability in nutrients using Michaelis-Menten relationships. Diatoms
324 differ from nanophytoplankton by their need in silicon, by higher requirements in iron
325 (Sunda and Huntsman, 1997) and by higher half-saturation constants because of their
326 larger mean surface-to-volume aspect ratio. Zooplankton is represented by two size-
327 classes: microzooplankton and mesozooplankton.

roland seferian 23/10/15 19:59

Deleted: to

328 PISCES can be considered as a Monod model (Monod, 1942) since it does not
329 | represent the internal concentration of nutrients in the cells. The ratios between
330 carbon, nitrate and phosphate are kept constant to the values proposed by Takahashi et
331 al. (1985) in all living and nonliving pools of organic matter. However, internal
332 concentrations of iron in both phytoplankton and of silicon in diatoms are
333 prognostically simulated. They depend on the external concentration of these
334 nutrients, on the potential limitation by the other nutrients and on light availability.

roland seferian 23/10/15 20:00

Deleted: to

335 Phytoplankton chlorophyll concentration is prognostically simulated following Geider
336 | et al. (1998). PISCES simulates semilabile dissolved organic matter, small and big
337 sinking particles, which differ by their sinking speeds (i.e., 3 m d⁻¹ and 50 to 200 m d⁻¹)

roland seferian 23/10/15 20:01

Deleted: formulation

338 ¹, respectively). Only the internal concentrations of iron, silicon and calcite inside the
339 sinking particles are prognostically simulated. In addition to exchange with organic
340 carbon, dissolved inorganic carbon is also altered by the production and dissolution of
341 calcite. Carbon chemistry in seawater is computed from the distribution of dissolved
342 inorganic carbon and alkalinity. Calcite is prognostically simulated following Maier-
343 Reimer, (1993) and Moore et al. (2002). Alkalinity includes the contribution of
344 carbonate, bicarbonate, borate and water ions. Oxygen is prognostically simulated
345 using two different oxygen-to-carbon ratios, one accounting when ammonium is
346 converted to or mineralized from organic matter, the other when oxygen is consumed
347 during nitrification. For carbon and oxygen pools, air-sea exchange follows the
348 Wanninkhof (1992) formulation. Importantly, to ensure conservation of nitrogen in
349 the ocean, annual total nitrogen fixation is adjusted to balance losses from
350 denitrification following Lipschultz et al. (1990), Middelburg et al. (1996) and
351 Soetaert et al. (2000). For the other macronutrients, alkalinity and organic carbon, the
352 conservation is ensured by tuning the sedimental loss to the total external input from
353 rivers and dust. Therefore, carbon and nitrogen cycles are decoupled to a certain
354 degree.

355 The boundary conditions account for nutrient supply from three different sources:
356 atmospheric dust deposition for iron and silicon (Jickells and Spokes, 2001; Moore et
357 al., 2004; Tegen and Fung, 1995), rivers for carbon (Ludwig et al., 1996) and
358 sediment mobilization for sedimentary iron (de Baar and de Jong, 2001; Johnson et
359 al., 1999). In CNRM-ESM1, riverine input of carbon has been revised from Ludwig et
360 al. (1996) in accounting for the interannual variability of runoff estimated with an
361 offline SURFEX simulation over the 1948-2010 period using the global atmospheric
362 forcing from Princeton University (PGF, Sheffield et al., 2006).

363 In CNRM-ESM1, the marine biophysical feedback is induced by changes in the
364 penetration of downward irradiance in response to marine biota chlorophyll
365 concentration. This feedback mimics the fact that light absorption in the ocean indeed
366 depends on particle concentration and is spectrally selective (Morel, 1988). The
367 implementation of this mechanism is fully described in Lengaigne et al. (2006) and
368 Lengaigne et al. (2009) for an ocean forced configuration and Mignot et al. (2013) for
369 a current ocean coupled configuration. It is derived from an accurate 61 spectral bands

roland seferian 23/10/15 17:25

Formatted: Font:12 pt

roland seferian 23/10/15 17:25

Formatted: Font:12 pt

roland seferian 23/10/15 17:25

Formatted: Font:12 pt

roland seferian 23/10/15 17:25

Deleted: to ensure conservation of nitrate in the ocean, annual total nitrogen fixation should balance denitrification

roland seferian 23/10/15 17:25

Deleted: following Lipschultz et al. (1990), Middelburg et al. (1996) and Soetaert et al. (2000).

roland seferian 23/10/15 17:25

Formatted: Font:12 pt

roland seferian 23/10/15 17:23

Deleted:

roland seferian 23/10/15 20:04

Deleted: with

roland seferian 10/12/15 19:54

Formatted: Font:12 pt

roland seferian 10/12/15 19:54

Formatted: Font:12 pt, Font color: Black, English (US)

roland seferian 23/10/15 20:04

Deleted: Princeton atmospheric forcing. .

roland seferian 10/12/15 19:54

Formatted: Font:Font color: Black

370 formulation proposed by Morel (1988) using three large wavebands: blue (400–500
371 nm), green (500–600 nm) and red (600–700 nm). These three bands correspond to the
372 spectral domain of maximum absorption for chlorophyll. The chlorophyll-dependent
373 attenuation coefficients depend on the three-dimensional chlorophyll field predicted
374 by PISCES. They are computed at each time step from a power-law relationship
375 fitting to the coefficients computed from the full spectral model of Morel et al. (1988).
376 This biophysical feedback represents a major evolution from the ocean component
377 used in Voldoire et al. (2013) and Séférian et al. (2013).

378

379 3- Experimental set-up

380 3-1 Spin-up strategy

381 The CMIP5 specification requires each model to reach its equilibrium state before
382 kicking off formal simulations, especially for long-term control experiments. To
383 obtain the initial conditions for CNRM-ESM1 preindustrial steady state at year 1850,
384 we first initialize the various physical and biogeochemical components of the model
385 as described below and perform a 400-year-long spin-up simulation using CNRM-
386 ESM1 with all 1850 external forcings (Taylor et al., 2009).

387 Initialization of the physical components of CNRM-ESM1 relies on previous model
388 outputs from CNRM-CM5.1. This latter model was first initialized from World Ocean
389 Atlas 2005 observations for salinity and temperature (Antonov et al., 2006; Locarnini
390 et al., 2006) and spun-up for 200 years. The 801th year of the centennial long CMIP5
391 preindustrial run from CNRM-CM5.1 was employed as initial condition for CNRM-
392 ESM1 preindustrial state.

393 Marine biogeochemical reservoirs were initialized from fields of a previous
394 preindustrial simulation of CNRM-CM5.1 coupled to PISCES. In this previous
395 simulation, PISCES state variables were initialized from World Ocean Atlas 1993
396 observations for nitrate, phosphate, silicate, and oxygen (Levitus et al., 1993) and the
397 Global Ocean Data Analysis Project (Key et al., 2004) for alkalinity and preindustrial

roland seferian 23/10/15 17:27

Deleted: Equilibrium

roland seferian 23/10/15 17:34

Deleted: 32

roland seferian 23/10/15 17:34

Deleted:

roland seferian 23/10/15 17:29

Deleted: online

398 dissolved inorganic carbon (DIC). From this initialization, this intermediate version of
399 the ESM was integrated online for 1100 years.

400 Land biogeochemical reservoirs were initialized from zero and spun-up using an
401 acceleration approach for soil carbon and wood during the first century of the spin-up
402 simulation. This approach consists in updating the wood growth, the litter and soil
403 biogeochemistry modules several times per time step with constant incoming carbon
404 fluxes and physical conditions allowing to fill up much faster the various reservoirs of
405 carbon. As a result of this approach, soil carbon and wood reservoirs were
406 respectively spun-up for 21800 and 1200 years.

roland seferian 23/10/15 17:31

Deleted: on-line

407 Finally, both physical and carbon cycle components of CNRM-ESM1 benefit from an
408 physical adjustment under 1850 preindustrial control conditions for 400 years. Section
409 4.1 describes the residual drifts of the model at quasi-equilibrium state.

roland seferian 23/10/15 17:34

Deleted: on-line

410

411 3-2 CMIP5 preindustrial control and historical simulations

412 Following CMIP5 specifications (Taylor et al., 2009), CNRM-ESM1 has performed
413 several CMIP5 long-term core experiments and part of the tier-1 experiments.

414 The preindustrial control simulation, *piControl*, is integrated for 250 years using
415 constant external forcing prescribed at 1850 conditions and starting from the last year
416 of the on-line adjustment simulation. That is, atmospheric concentrations of
417 greenhouse gases are set to 284.7 ppmv, 790.9 ppbv, and 275.4 ppbv for CO₂, CH₄
418 and N₂O, respectively. Those of CFC-11, CFC-12 are set to zero. Influence of natural
419 aerosols is prescribed using the optical depths of five types of tropospheric aerosols
420 (black carbon, sea salt, sulfate, dust and particle organic matter) from an LMDZ-
421 INCA simulation forced with CMIP5 prescribed emissions (Szopa et al., 2013).
422 Stratospheric volcanic aerosols are prescribed similarly but using a long-term average
423 climatology from a last millennium simulation performed with the NCAR Community
424 Climate System Model (Ammann et al., 2007).

roland seferian 23/10/15 17:39

Formatted: Font:12 pt

roland seferian 23/10/15 17:38

Deleted: the NCAR model

425 The 20th century experiment, *historical*, is performed from year 1850 to 2005. This
426 simulation starts from the CNRM-ESM1 states of the last year of the on-line

427 adjustment simulation. The modern evolution of the external forcings of both
428 atmospheric greenhouse gases and incoming solar irradiance follows the
429 recommended yearly average observations (Taylor et al., 2009). The monthly
430 temporal and spatial variability of the five tropospheric aerosols also rely on a LMDZ-
431 INCA simulation (Szopa et al., 2013) while those of stratospheric sulphate aerosol
432 concentrations from explosive volcanoes are derived from a 20th century
433 reconstruction of [the NCAR Community Climate System Model \(Ammann et al.,](#)
434 [2007\)](#).

roland seferian 10/12/15 19:51
Deleted: the NCAR model (Ammann et al.,
2003)

435 Note there is no land-cover change related to anthropogenic land use in the above-
436 mentioned simulations. The fraction of vegetal cover is set to the present-day state
437 using the in-house ECOCLIMAP database (Masson et al., 2013a). Therefore, changes
438 in physical and biogeochemical properties of the vegetation due to actual land-cover
439 changes are excluded by design.

440

441 **4- Results**

442 **4-1 Model equilibrium in the preindustrial control simulation**

443 To illustrate the stability of CNRM-ESM1 at the end of the spin-up simulation, we
444 show the global average values of a few variables during the 250 years of the
445 piControl simulation (Figure 2) and their drifts (Table 1).

446 In terms of energy balance, the global mean top-of-atmosphere (TOA) net radiative
447 balance is about $3.57 \pm 0.23 \text{ W m}^{-2}$, while the global mean net surface radiation flux
448 (NSF) is $0.87 \pm 0.24 \text{ W m}^{-2}$ (Figure 2a). The imbalance in the energy budget between
449 the surface and TOA (about 2.7 W m^{-2}) is predominantly due to the non-conservation
450 of energy of the spectral atmospheric model and, to a lesser extent, its coupling with
451 the ocean model. Taking apart this non-conservation offset in TOA net radiation flux,
452 there is no discernible deviation between year-to-year fluctuation between the TOA
453 and NSF net radiation fluxes.

454 In terms of global-scale climate indices, the global mean surface temperature (T_{2m})
455 and sea surface temperature (SST) over the piControl period are 12.52 ± 0.15 and

456 17.76±0.1°C respectively (Figure 2b). They both display almost no drift over the
457 duration of the piControl simulation (Table 1). We use soil wetness index (SWI) and
458 sea surface salinity (SSS) to evaluate the stability of the simulated water cycle (Figure
459 2c). These both have almost no drift (Table 1), confirming that the water cycle is
460 closed. Also, there is no drift in both Northern Hemisphere and Southern Hemisphere
461 sea-ice volume (NIV, SIV, respectively) for which long-term means are respectively
462 20.88 and 6.25 10³ km³ (Figure 2d).

463 Regarding the simulated global carbon cycle, Figure 2e shows that the natural carbon
464 cycle is stable over the piControl simulation with terrestrial and oceanic carbon fluxes
465 of 0.75±0.57 and -0.94±0.13 Pg C y⁻¹, respectively. Both terrestrial and oceanic
466 components of the simulated carbon cycle exhibit drifts smaller than 10⁻³ Pg C y⁻¹
467 demonstrating that soil and deep ocean carbon stocks have reached a steady state.
468 Deviation from zero in the terrestrial carbon flux is essentially explained by missing
469 perturbations or processes in ISBA such as fire-induced CO₂ emissions or riverine-
470 induced carbon transport from land to oceans (Battin et al., 2009; Regnier et al.,
471 2013). Natural ocean carbon outgassing falls within the upper range of ocean inverse
472 estimates (Jacobson et al., 2007; Mikaloff Fletcher et al., 2007).

473

474 **4-2 Late 20th century climatology**

475 **4-2-1 Land physical drivers**

476 In the following, we focus on the physical drivers of the global carbon cycle. From a
477 land perspective, surface temperature (T_{2m}), precipitation (PR) and photosynthetically
478 active radiation (PAR) are the prominent factors controlling the rate of photosynthetic
479 activity as well as the rate of autotrophic and heterotrophic respiration, and hence the
480 net land-air exchange of carbon.

481 Compared to the CRUTV4 dataset (Harris et al., 2013) over the period 1986-2005,
482 CNRM-ESM1 displays a global annual averaged bias of -3°C in T_{2m} over continents.
483 In Northern Hemisphere winter (DJFM, Figure 3a) simulated T_{2m} is generally lower
484 than the observations except for some regions (e.g., North East Siberia, South of

roland seferian 23/10/15 17:57

Formatted: Subscript

roland seferian 23/10/15 17:56

Deleted: the weathering and

485 Australia and part of Argentina). The mean bias over continents in boreal winter is
486 about -4°C and can reach up to -6°C over mountain regions. Figure 3b shows that
487 simulated summer (i.e., JJAS) T_{2m} is also generally colder than the observations ($-$
488 0.8°C in global average) over a large fraction of the continents. Only the most
489 Northern domains of the Northern Hemisphere display a warm bias that can reach up
490 to 3°C in the North of Canada. The geographical structure of the T_{2m} bias compares
491 well with those detailed in Voldoire et al. (2013). Such an agreement in the bias
492 structure for T_{2m} was expected since both models rely on the same physical
493 parameterizations for both the atmosphere and land surface physics. Small deviations
494 between CNRM-CM5 and CNRM-ESM1 mean state can be essentially attributed to
495 the land carbon cycle, which appears to amplify the global average annual cold bias of
496 0.8°C (with seasonal differences between CNRM-ESM1 and CNRM-CM5 of -0.7°C
497 and -1°C in boreal winter and summer, respectively). This cooling is due to the
498 enhanced evapotranspiration by the interactive terrestrial biosphere compared to the
499 fixed one in CNRM-CM5.

roland seferian 23/10/15 20:06

Deleted: (

roland seferian 23/10/15 20:06

Deleted: ,

roland seferian 23/10/15 18:01

Deleted: average

roland seferian 23/10/15 18:01

Deleted: biases

500 Figure 4 shows the regional structure of the precipitation (PR) bias of CNRM-ESM1
501 with respect to the Global Precipitation Climatology Project (GPCP) observations
502 (Adler et al., 2003). Over continents, CNRM-ESM1 slightly underestimates the
503 amount of the seasonal PR except over Asia, the Western coast of America and
504 Australia. The major regional bias in seasonal PR is found over Amazonia, where PR
505 is underestimated by 2 and 5 mm day^{-1} in boreal summer and winter, respectively.
506 Similar to state-of-the-art Earth system models, CNRM-ESM1 displays an excess of
507 precipitation over the oceans. This excess is especially strong in the Southern part of
508 the tropical oceans and is associated with the overestimated seasonal latitudinal
509 migration of the ITCZ. The land biosphere biophysical coupling induces small but
510 noticeable changes in the global hydrological cycle between CNRM-CM5 and
511 CNRM-ESM1. Although weak, changes induced by the ISBA biophysical coupling
512 slightly affect the representation of the seasonal cycle in PR over the vegetated
513 regions (Figure S1). These lead to improve the simulated PR in CNRM-ESM1
514 compared to CNRM-CM5 over some vegetated regions during the growing season
515 (spring-summer). Between 30°N and 60°N , the average error in simulated PR
516 compared to GPCP is reduced by 0.12 mm day^{-1} with CNRM-ESM1 compared to that
517 of CNRM-CM5. Over the tropics (30°S - 30°N), simulated PR is also improved in

roland seferian 23/10/15 20:07

Formatted: Font:Not Bold

roland seferian 23/10/15 20:07

Deleted: GPCP

roland seferian 30/11/15 17:33

Formatted: Font:12 pt, Font color: Auto, English (US)

roland seferian 30/11/15 17:33

Formatted: Font color: Auto

roland seferian 30/11/15 17:33

Formatted: Font:12 pt, Font color: Auto, English (US)

roland seferian 30/11/15 17:33

Formatted: Font:12 pt, Font color: Auto, English (US)

roland seferian 30/11/15 17:33

Formatted: Font:12 pt, Font color: Auto, English (US)

518 CNRM-ESM1 but to a lesser extent with a reduction of the average error by 0.06 mm
519 day⁻¹ with respect to GPCP. Although PR have been improved over some regions,
520 their geographical pattern has been degraded in CNRM-ESM1 compared to CNRM-
521 CM5, especially during the winter.

522 Compared to SRB satellite-derived observations (Pinker and Laszlo, 1992), CNRM-
523 ESM1 overestimates the photosynthetically active radiation (PAR) globally (Figure
524 5). Major biases are found over continents except for some regions in the Tropics. The
525 magnitude of the seasonal biases is weaker in Northern Hemisphere winter than in
526 summer when regional biases reach up to 20-30 W m⁻² over the Western border of the
527 continents. Regions where PAR is underestimated match reasonably well with those
528 showing too intense precipitations compared to the GPCP dataset (Figure 4). The
529 general overestimation in PAR is due to the substantial underestimation in low cloud
530 cover in CNRM-ESM1 consistent with CNRM-CM5. Biases in PAR are also found
531 over ocean upwelling system and are linked with an underestimated fraction of
532 stratocumulus.

533

534 4-2-2 Ocean physical drivers

535 From an oceanic perspective, temperature is as important as over land surface because
536 it sets the marine biota's growth rate, playing a large role in the biological-mediated
537 processes (e.g., export, soft tissue pump). In addition, both temperature (T) and
538 salinity (S) control the solubility of CO₂ into seawater and the chemical-mediated air-
539 sea exchanges of carbon. The mixed-layer depth (MLD) and the sea-ice cover (SIC)
540 are also critical drivers of the ocean carbon cycle as they both contribute to the
541 nutrient-to-light limitation in the high latitude oceans (Sarmiento and Gruber, 2006).
542 In the following, we assess the representation of these drivers.

543 Compared to WOA2013 data products (Levitus et al., 2013), CNRM-ESM1
544 realistically simulates both the mean annual sea surface temperature and sea surface
545 salinity, both in terms of amplitude and spatial distribution, as shown in Figure 6ab.
546 Moderate positive biases in sea surface temperature and sea surface salinity are found
547 in the Southern Ocean and in the Eastern boundary upwelling systems. Strong biases

roland seferian 30/11/15 17:33
Formatted: Font:12 pt, Font color: Auto, English (US)

roland seferian 30/11/15 17:33
Formatted: Font:12 pt, Font color: Auto, English (US)

roland seferian 30/11/15 17:33
Formatted: Font:12 pt, Font color: Auto

roland seferian 30/11/15 17:33
Formatted: Font:12 pt, Font color: Auto, English (US)

roland seferian 30/11/15 17:33
Formatted: Font:12 pt, Font color: Auto

roland seferian 30/11/15 17:33
Formatted: Font:12 pt, Font color: Auto, English (US)

roland seferian 30/11/15 17:30
Formatted: English (US)

548 in sea surface salinity are found in the Labrador and Arctic Seas. While most of these
549 biases are related to an overestimated atmospheric surface heating, biases in the
550 Labrador Sea and in the Arctic are essentially due to erroneous representation of the
551 mixed-layer depth and the Arctic sea-ice cover. These points will be further detailed
552 below.

553 At depth, the vertical structures in simulated T and S display biases from those
554 estimated from WOA2013 observations. T is underestimated by $\sim 2^{\circ}\text{C}$ within the first
555 1000 m of the Atlantic and Pacific oceans, except in the deep water formation zone
556 (North Atlantic, North Pacific and Southern Ocean), where the model displays
557 positive biases. The largest deviation in vertical structure of simulated S from that
558 estimated from WOA2013 are found in deep water formation zones where haline
559 biases of about ~ 1 psu tend to compensate for the warm bias in T, enabling deep
560 convection of water masses. Because of this compensating mechanism, the flow of
561 North Atlantic deep waters (NADW) fueling the Atlantic meridional overturning
562 circulation is about 26.1 ± 2 Sv at 26.5°N in CNRM-ESM1 averaged over the 1850-
563 2005 period. This value is stronger than the observations-derived estimate of 18 ± 5
564 Sv (Talley et al., 2003) or the observations from RAPID-MOCHA monitoring array
565 over 2004-2007 estimating the flow at about 18.5 ± 4.9 Sv (Johns et al., 2011). In the
566 Southern Ocean, the flow of Antarctic bottom water (AABW) is about 11.6 ± 1 Sv in
567 CNRM-ESM1 averaged over the 1850-2005 period. This flow of AABW is in
568 agreement with the deep flow of waters compared to the observed estimate of 10 ± 2
569 Sv (Orsi et al., 1999). Consequently, the flow of deep water masses in CNRM-ESM1
570 has been improved in regards that of CNRM-CM5 which ranges between 3.4 and 6.2
571 Sv over the same period (Séférian et al., 2013; Voltaire et al., 2013). As detailed in
572 several intercomparison studies (de Lavergne et al., 2014; Heuzé et al., 2013; Sallée et
573 al., 2013; Séférian et al., 2013), CNRM-CM5 substantially underestimated the flow of
574 AABW leading to an erroneous distribution of hydrodynamical and biogeochemical
575 fields at depth. Here, although stronger than the observation-based estimates, the flow
576 of NADW and AABW improves the deep ocean ventilation as well as the distribution
577 of tracers at depth (section 4-2-5).

578 As mentioned above, an accurate representation of spatial and temporal MLD is
579 essential for numerous ocean biogeochemical processes. For example, winter mixing

roland seferian 20/2/16 11:52

Deleted: present moderate

roland seferian 20/2/16 11:53

Deleted: deviation

roland seferian 20/2/16 11:55

Deleted: Contrasting to T, the

roland seferian 20/2/16 11:56

Deleted: matches well with WOA2013 observations. Deviations

roland seferian 20/2/16 11:56

Deleted: e

roland seferian 20/2/16 11:56

Deleted: observed S profile

roland seferian 20/2/16 17:07

Deleted: Thanks to

Unknown

Field Code Changed

roland seferian 27/11/15 11:00

Deleted: is stronger

roland seferian 27/11/15 16:05

Formatted: Not Highlight

roland seferian 27/11/15 11:01

Deleted: than

roland seferian 27/11/15 16:05

Formatted: Not Highlight

roland seferian 27/11/15 16:05

Formatted: Not Highlight

roland seferian 27/11/15 16:05

Formatted: Not Highlight

roland seferian 27/11/15 11:02

Deleted:

Unknown

Field Code Changed

580 entrains carbon- and nutrient-rich deep waters to the surface, which play an important
581 role in the transfer of CO₂ across the sea-to-air interface. In summer, MLD contributes
582 to the nutrient-to-light limitation of the phytoplankton growth in high-latitude oceans.
583 The maximum and minimum mixed-layer depth (hereafter, MLD_{max} and MLD_{min}) are
584 respectively used as a proxy of the winter and summer MLD since mixing occurs
585 randomly during seasons in response to numerous environmental factors (wind,
586 stratification, local instability etc...) that present a large spatiotemporal variability.
587 Figure 7 presents composites of yearly MLD_{max} and MLD_{min} as simulated by CNRM-
588 ESM1 in averaged over the 1986-2005 period and as derived from observations
589 (Sallée et al., 2010). Figure 7ab shows that CNRM-ESM1 reproduces the main
590 regional pattern of MLD_{max} compared to the observation-derived estimates. However,
591 the model tends to simulate too large and too deep mixing sites in the North Atlantic,
592 the North Pacific and the Southern Ocean. In the North Atlantic, the larger than
593 observed mixed volume of surface dense waters (combination of surface area and
594 depth of the mixing zone) is at the origin of the strong flow of NADW simulated in
595 CNRM-ESM1. In the Southern Ocean, although open ocean polynyas were observed
596 from space in the past decades (Cavaleri et al., 1996; Comiso, 1999), their locations
597 are erroneous in CNRM-ESM1 similarly to several other CMIP5 Earth system models
598 (de Lavergne et al., 2014). CNRM-ESM1 simulates open ocean polynyas in the Indian
599 basin and close to the Ross Sea but not in the Atlantic basin as observed from space
600 between 1974 and 1976.

601 Compared to the observation-derived estimates, CNRM-ESM1 captures the main
602 regional pattern of MLD_{min} but the model fails at reproducing the deepest values of
603 mixing in the Southern Ocean and the Tropics. This bias might be linked to the
604 current parameterization of the ocean mixing employed in CNRM-ESM1 because
605 previous model version using this parameterization also exhibited similar patterns of
606 errors as detailed in S  ferian et al. (2013) and Voldoire et al. (2013).

607 Similarly to the MLD, SIC is an important driver of the ocean carbon cycle. It
608 constitutes a physical barrier for exchange of CO₂ between the ocean and the
609 atmosphere leading to an accumulation of carbon-rich waters below the sea ice
610 (Takahashi, 2009). It also plays a large role in the seasonal timing of algal blooms
611 (Wassmann et al., 2010). Compared to the MLD, seasonal variations of sea ice are

roland seferian 20/2/16 17:10

Deleted:

roland seferian 23/10/15 18:11

Deleted: over the 1986-2005 period

roland seferian 20/2/16 12:01

Deleted: well

roland seferian 23/10/15 20:38

Deleted: Interestingly, CNRM-CM5 did not present such erroneous location of the open ocean polynyas as documented in Voldoire et al. (2013) and further investigated in de Lavergne et al. (2014). The use of GELATO6 in CNRM-ESM1 compared to GELATO5 in CNRM-CM5 in addition to the change in coupling frequency might be at the origin of this model-data disagreement. .

roland seferian 20/2/16 12:11

Deleted: the

roland seferian 20/2/16 12:11

Deleted: is reasonably well simulated in CNRM-ESM1. Compared to the previous model versions (S  ferian et al., 2013; Voldoire et al., 2013),

roland seferian 20/2/16 12:11

Deleted: CNRM-ESM1

roland seferian 20/2/16 12:12

Deleted: ese are tightly linked to

roland seferian 20/2/16 12:18

Deleted: implying a contribution of the surface wind energy to the mixing below the MLD

roland seferian 20/2/16 12:06

Deleted: .

612 strongly and directly responsive to the seasonal fluctuations of atmospheric forcing.
613 Therefore, it matters that the model is able to accurately capture the spatial
614 distribution and timing of annual minimal and maximal sea ice covers in both
615 Hemispheres. For this purpose, we evaluate differences between composites of
616 simulated and observed SIC (Cavalieri et al., 1996) for September and March over the
617 1986-2005 period (Figure 8). In the Arctic Ocean, CNRM-ESM1 underestimates SIC
618 in the Beaufort, Chukchi and East Siberian seas in September, while too much sea ice
619 tends to be present in the Barents Sea (Figure 8a). In March, SIC is largely
620 overestimated in the Barents and Nordic seas, as well as in the Bering and Okhotsk
621 seas on the Pacific Ocean side, showing that the simulated winter sea ice edge spreads
622 too far South and East in these regions (represented with iso-15% in Figure 8c). On
623 the contrary, SIC is slightly underestimated in the Labrador Sea and Baffin Bay in
624 March (Figure 8c). This too far North ice edge comes along with positive SST biases
625 in this region (Figure 6a), and explains why the simulated deep convection zone is too
626 large and shifted northward in CNRM-ESM1 as shown in Figure 7.

627 In the Antarctic Ocean, Figure 8b shows that the spatial structures of SIC biases
628 mirror somehow the model-data mismatch in MLD as shown in Figure 7b. That is, in
629 austral winter, CNRM-ESM1 underestimates SIC where erroneous open ocean deep
630 convection zones are located, namely offshore Wilkes Land in the Indian Ocean
631 sector (Figure 8b). Conversely, too much sea ice is simulated in the Atlantic Ocean
632 sector. As in CNRM-CM5.1, simulated summer Antarctic SIC is strongly
633 underestimated, with very little sea ice surviving summer melt in the Weddell and
634 Ross Seas (Figure 8d).

635

636 4-2-3 Comparison with previous model version

637 In the following, we compare the skill of CNRM-ESM1 to the closest version of
638 CNRM-CM5 climate model, called CNRM-CM5.2. Figure 9 summarizes skill-
639 assessment metrics for CNRM-ESM1 and CNRM-CM5.2 in terms of major physical
640 drivers of the global carbon cycle (field maps and patterns of errors are presented in
641 Figures S2 to S7).

roland seferian 23/10/15 20:08

Deleted: -

roland seferian 23/10/15 20:08

Deleted: -

roland seferian 21/2/16 10:05

Deleted: .

642 The Taylor diagram for land surface physical drivers clearly demonstrates that
643 CNRM-ESM1 and CNRM-CM5 display comparable skills except for PR (Figure 9a).
644 Most of the differences in skills are indeed not significant at a 95% confidence level;
645 models differ solely in terms of PR for which CNRM-ESM1 produces slightly weaker
646 correlation coefficients.

647 Over the ocean, Figure 9b shows further differences between both models. The
648 weakest difference in skill concerns SST for which both models display good
649 agreement with WOA2013. Regarding the MLD, CNRM-ESM1 displays a slightly
650 better agreement than CNRM-CM5.2 with observation-derived MLD (Sallée et al.,
651 2010) in terms of correlation but strongly underestimates the spatial variations of this
652 field. Major differences are noticeable for SSS. CNRM-ESM1's skill is clearly lower
653 than that of CNRM-CM5.2. To investigate this difference, we have computed skill of
654 PR over the ocean since this latter contributes to the spatiotemporal distribution of the
655 SSS concomitantly to the runoff and the sea-ice seasonal cycle. Skill in PR over the
656 ocean is similar for both models (blue diamonds on Figure 9b). A similar finding is
657 noticed for simulated runoff (not shown). Therefore the difference in simulated SSS
658 between the two models can be attributed to the revised water conservation interface
659 and erroneous distribution of sea-ice cover. In addition, changes in coupling
660 frequency (i.e. 24h to 6h) might be at the origin of differences in skills between the
661 two models since it impacts sea-ice cover (Figure 10).

662 From the small differences in skill between the two models, we can assume that the
663 inclusion of the global carbon cycle and the biophysical coupling have not noticeably
664 altered the simulated mean-state climate in CNRM-ESM1 compared to that of
665 CNRM-CM5.2.

666

667 4-2-4 Terrestrial carbon cycle

668 Now that the physical drivers of the global carbon cycle have been evaluated, we
669 assess the ability of CNRM-ESM1 to replicate available modern observations of the
670 terrestrial carbon cycle. We focus on gross primary productivity (GPP), vegetation
671 autotrophic respiration (Ra) and soil organic carbon content (cSoil) that control the

roland seferian 23/10/15 20:08

Deleted: -

roland seferian 1/12/15 12:14

Deleted: over

roland seferian 23/10/15 20:09

Deleted: -

roland seferian 2/12/15 12:33

Deleted: (supplementary materials)

roland seferian 2/12/15 12:33

Deleted: Besides

roland seferian 23/10/15 20:09

Deleted: -

672 net natural fluxes of CO₂ on land. Simulated budget of vegetation biomass and total
673 ecosystem respiration (TER, sum of autotrophic and heterotrophic respirations) are
674 evaluated against available published estimates. While we can assess the capability of
675 CNRM-ESM1 to fix and emit carbon on land, it is important to note that the CO₂
676 fluxes due to land-use changes are not taken into account in this analysis.

677 To evaluate CNRM-ESM1 GPP, we rely on two streams of data, namely the FluxNet-
678 MTE (Jung et al., 2011) and the MOD17 satellite-derived observations (Running et
679 al., 2004). Figure 1 shows that the annual mean GPP as simulated by CNRM-ESM1
680 is slightly too strong compared to the observed estimates. The largest model-data
681 mismatch is found in the Tropics between 10°N and 20°S, where CNRM-ESM1
682 simulates erroneous patterns of high GPP. Over Amazonia, CNRM-ESM1 fails to
683 reproduce the zonal gradient of GPP. Regions of high GPP are in association with
684 overestimated PAR and, to a lesser extent, underestimated PR in summer (Figure 4
685 and Figure 5, respectively; [see also Figure S8](#)). The geographical structure of
686 simulated GPP fits the observed over the African and Asian rain forest but its
687 amplitude is overestimated by about 3 gC m⁻² day⁻¹. This regional overestimation
688 impacts both the zonal and global GPP budget, which are larger than the published
689 estimates except >60°N (Table 2). This stronger-than-observed GPP constitutes a
690 systematic bias of the current version of ISBA. In an offline simulation, (Carrer et al.,
691 2013b) show that ISBA forced with [PGF](#) overestimates global GPP by 60 Pg C y⁻¹.
692 Regional biases in GPP are partly compensated by overestimated Ra (Figure 12).
693 Simulated Ra agrees reasonably well with satellite-derived estimates except in the
694 Tropics. This bias compensation between GPP and Ra is analyzed in detail by Joetzjer
695 et al. (2015). In this study, the authors demonstrate that the current parameterizations
696 of Ra and water stress in ISBA are not adequate for tropical broadleaf trees ([Figure 1](#)).
697 Considering that these results were deduced from offline simulations forced with in
698 situ observations, we can assume here that biases in GPP and Ra result from a
699 combination of erroneous ecophysiological parameterizations and biases in physical
700 drivers in CNRM-ESM1.

701 Despite these biases, the global partitioning between vegetation biomass and soil
702 carbon is realistic with 596.7 and 2105 Pg C compared to the observed estimates of
703 560±94 (DeFries et al., 1999) and 1750±250 Pg C (Houghton, 2007), respectively.

roland seferian 2/12/15 12:35

Deleted: 0

roland seferian 23/10/15 20:10

Deleted: amplitude of

roland seferian 23/10/15 20:10

Deleted: (values)

roland seferian 20/2/16 17:18

Deleted: d

roland seferian 23/10/15 19:32

Deleted:

roland seferian 23/10/15 19:32

Deleted: supplementary material

roland seferian 23/10/15 20:11

Comment: Sheffield et al., 2006

roland seferian 26/10/15 14:33

Deleted: Princeton university forcings

roland seferian 26/10/15 14:33

Formatted: Not Highlight

roland seferian 26/10/15 14:33

Deleted: (REF)

roland seferian 2/12/15 12:36

Deleted: 1

704 Furthermore, the geographical structure of cSoil agrees well with Harmonized World
705 Soil Database (JRC, 2012) except in the Northern Hemisphere (Figure 13). Although
706 several processes are missing in ISBA to accurately simulate high-latitude carbon
707 stock (e.g., permafrost dynamics, bacterial degradation of the litter, fire-induced
708 turnover etc...), a part of cSoil underestimation can be attributed to the summer warm
709 bias in near-surface temperature (Figure 3b). This latter tends to enhance
710 heterotrophic respiration of the soil, reducing the soil organic matter ($R > 0.6$, Figure
711 S2).

roland seferian 2/12/15 12:36

Deleted: 2

712 Table 2 shows that CNRM-ESM1 overestimates globally terrestrial ecosystem
713 respiration (TER) when compared to the up-scaled measurements of FluxNet-MTE. In
714 the Tropics, simulated TER fluxes are 32% higher than the FluxNet-MTE estimates.
715 As mentioned above, this bias is essentially due to an unrealistic R_a , which amounts
716 to 72% of TER over the sector in the model. Table 2 shows that the simulated TER is
717 $126.9 \text{ Pg C y}^{-1}$, larger than estimates published by Jung et al. (2011) of $96.4 \pm 6.0 \text{ Pg C}$
718 y^{-1} . Nevertheless, the simulated net land carbon sink (LCS), which can be estimated
719 by subtracting TER from GPP, is 2.19 Pg C y^{-1} in average over the 1986-2005 period
720 and remains within the range of values estimated from various observation-based
721 methods (IPCC, 2007; 2013; Le Quéré et al., 2014).

roland seferian 23/10/15 19:32

Deleted: supplementary materials

roland seferian 20/2/16 17:24

Deleted: compared to

roland seferian 23/10/15 20:13

Deleted: and

722

723 4-2-5 Ocean carbon cycle

724 Compared to the terrestrial carbon cycle, the ocean carbon cycle has already been
725 implemented in previous versions of CNRM-CM5 (Séférian et al., 2013). The
726 modeled marine biogeochemistry components have already benefited from detailed
727 evaluation against modern observations (Frölicher et al., 2014; Séférian et al., 2013),
728 analyses of future projections (Laufkötter et al., 2015) and sensitivity benchmarking
729 (Schwinger et al., 2014). The major difference between CNRM-ESM1 and previous
730 versions of CNRM-CM5 including a marine biogeochemistry module lies in the
731 representation of ocean tracers in the deep ocean. Figure 14 shows that the
732 representation of oxygen, phosphate, nitrate and silicate fields was improved in
733 CNRM-ESM1 at depth, except around 1000 m where the strong flow of NADW tends
734 to alter the distribution of tracers. Below 1500 m, the tracer distribution is in

roland seferian 2/12/15 12:36

Deleted: 3

735 reasonable agreement with the observations with correlation coefficients ~ 0.8 . This
736 represents a noticeable improvement with respect to the CNRM-CM5 oxygen
737 distribution ($R \sim 0.4$). In addition to nutrients, the vertical distribution of carbon-related
738 fields like dissolved inorganic carbon has been substantially improved in CNRM-
739 ESM1 compared to CNRM-CM5 (Figure S9), showing a much better agreement with
740 GLODAP observations (Key et al., 2004; Sabine et al., 2004).

roland seferian 23/10/15 19:33
Deleted: supplementary materials

741 In terms of carbon cycling into the ocean, Figure 15 shows the simulated mean annual
742 sea-air CO_2 fluxes over 1986-2005 together with observation-based estimates by
743 Takahashi et al. (2010) using 2000 as a single reference year. While the model
744 broadly agrees with the observations in terms of spatial variation for regions of carbon
745 sink (i.e., North Atlantic, North Pacific and between 50°S - 40°S), it displays a too
746 strong source of carbon to the atmosphere in the equatorial Pacific and in the Southern
747 Ocean. In the equatorial Pacific, the model-data mismatch is likely related to the
748 decision of Takahashi et al. (2010) to exclude observations from El Niño years from
749 their analysis. Since surface ocean pCO_2 of the Eastern tropical Pacific during El Niño
750 events tends to be lower than the long-term mean, the Lamont-Doherty Earth
751 Observatory (LDEO) climatology tends to underestimate outgasing of CO_2 in the
752 equatorial Pacific over the 1986-2005 period. This hypothesis is validated when
753 comparing model results against recent data products derived from statistical Monte-
754 Carlo Markov Chain or Neural Network gapfilling methods (Landschützer et al.,
755 2014; Majkut et al., 2014, Figure S10). In the Southern Ocean, the model-data
756 mismatch is especially pronounced south of 60°S . This bias in fgCO_2 is associated
757 with overestimated mixing (Figure 7), which tends to bring too much deep carbon-
758 rich water masses to the surface, enhancing the outgasing of CO_2 . CNRM-ESM1
759 results display similar discrepancy when compared to other recent observation-
760 derived data products which agree in a moderate CO_2 outgasing south of 60°S (Figure
761 S10). That said, simulated patterns of sea-to-air carbon fluxes in this domain
762 qualitatively agree with the data in showing a combination of source and sink regions.

roland seferian 2/12/15 12:37
Deleted: 4

roland seferian 2/12/15 20:36
Deleted: not shown

763 The storage of anthropogenic CO_2 by the oceans ($\text{CO}_2^{\text{ANTH}}$, Figure 16) provides a
764 complementary view of the ocean carbon fluxes by revealing the chronology of the
765 ocean CO_2 uptake from preindustrial to modern state. Here, we have chosen to stick to
766 the available observation-derived estimates, GLODAP, which use year 1994 as a

roland seferian 2/12/15 12:37
Deleted: 5

767 single reference year (Key et al., 2004; Sabine et al., 2004). In order to account for the
768 interannual variability of the simulated fields, we chose to analyze yearly average
769 results from CNRM-ESM1 over 1990-2005 (Figure 16). Besides, computation of
770 $\text{CO}_2^{\text{ANTH}}$ is not straightforward since natural and anthropogenic pools of carbon are not
771 treated separately in PISCES. We approximate consequently $\text{CO}_2^{\text{ANTH}}$ from the
772 difference between modern and preindustrial stocks of dissolved inorganic carbon.
773 Negative values were set to zero in the computation since they are essentially
774 generated from differences in simulated interannual variability. Ideally, this
775 computation would have required a historical simulation with constant preindustrial
776 atmospheric CO_2 for the sea-to-air CO_2 fluxes. Figure 16 shows that the maximum
777 $\text{CO}_2^{\text{ANTH}}$ is concentrated in the North Atlantic region. This feature is linked to the
778 large-scale circulation in the surface layer of the ocean, which converges in the North
779 Atlantic, before being exported to depth with the flow of NADW (Pérez et al., 2013).
780 The Southern Ocean also stores a large fraction of $\text{CO}_2^{\text{ANTH}}$ in association with the
781 subduction of modal and intermediate water masses (Sallée et al., 2012). Compared to
782 this global view, CNRM-ESM1 displays features that are broadly consistent with the
783 $\text{CO}_2^{\text{ANTH}}$ estimates. However, the stronger flow of NADW and AABW leads to a
784 depletion of the stock of $\text{CO}_2^{\text{ANTH}}$ between 0 and 1200 m (Figure 16c). This
785 mechanism leads to an increase in the stock of $\text{CO}_2^{\text{ANTH}}$ at depth. Over the 1850–1994
786 period, the model takes up a total of 100.8 Pg C, which is in agreement with the
787 observations that suggest a net uptake of 106 ± 17 Pg C over the same period
788 (Khatiwala et al., 2013; Sabine et al., 2004).

roland seferian 2/12/15 12:37

Deleted: 5

roland seferian 2/12/15 12:40

Deleted: 5

roland seferian 2/12/15 12:37

Deleted: 4

789

790 **4-2-6 Ecosystem dynamics**

791 In this section, we assess the performance of CNRM-ESM1 in terms of two
792 ecosystem dynamics parameters, namely the peak leaf area index (LAI_{max}) and the
793 ocean surface chlorophyll (Chl). Both parameters are monitored continuously from
794 space since the 1980s and the 1990s, respectively, providing a suitable set of indirect
795 observations to assess the simplified ecosystem representation embedded in Earth
796 system models.

797 | Regarding LAI_{max} , Figure 17 shows that the model agrees well with satellite-derived
798 observations (Zhu et al., 2013) except over Africa and Asia with overestimated
799 values. As such, this ecosystem parameter behaves similarly to GPP and Ra,
800 responding to biases in PR and PAR. In the Northern mid-latitudes, LAI_{max} is slightly
801 overestimated compared to the satellite-derived observations but remains in the low
802 range of values simulated by other CMIP5 Earth system models evaluated in Anav et
803 al. (2013b). Using an offline simulation forced with atmospheric reanalyzes (Szczypta
804 et al., 2014) shows similar biases in LAI over Northern Europe as those noticed in
805 CNRM-ESM1. It is thus likely that missing processes like forest and crop
806 management or fire-induced disturbance might induce an overestimated LAI_{max} .

roland seferian 2/12/15 12:38

Deleted: 6

807 | Regarding ocean Chl, Figure 18 shows that CNRM-ESM1 displays a reasonable
808 agreement with satellite-derived observations (O'Reilly et al., 1998). Although
809 regional patterns of Chl concentrations were improved compared to that of CNRM-
810 CM5 (Séférian et al., 2013), major model discrepancies are found in oligotrophic
811 gyres and equatorial upwellings. Biases are more pronounced in the Southern
812 Hemisphere where the model fails to produce very low Chl in the Southern Pacific
813 gyres. CNRM-ESM1 also fails at capturing Western border high Chl concentrations in
814 relation with the equatorial upwelling. Underestimated Chl concentrations in
815 upwelling systems are essentially due to biases in surface wind forcing but also to the
816 coarse horizontal and vertical resolution of the ocean model. This model limitation
817 partly explains why Chl concentrations are underestimated in high-latitude oceans. In
818 these domains, high coastal concentrations are captured from satellite sensors but
819 cannot be resolved by the model due to its coarse resolution.

roland seferian 2/12/15 12:38

Deleted: 7

820

821 4-3 Recent evolution of the Climate system

822 In the present section, we analyze the transient response of various climate indices to
823 the recent climate forcing from 1901 to 2005. We focus on the near-surface
824 temperature (T_{2m}), the September Arctic sea-ice extent (SIE), the 0-2000 m ocean heat
825 content (OHC) as well as the land and ocean carbon sinks (LCS, OCS, respectively).
826 Over this period, these climate indices are analyzed with their nominal values except
827 for T_{2m} and OHC that are represented with respect to the 1961-1990 and the 1955-

roland seferian 23/10/15 18:21

Deleted: change

828 | 2005 periods, respectively. Figure 19 illustrates how these various climate indices
829 | evolve from 1901 to 2005 and Table 3 summarizes their mean-state, interannual
830 | variability (IAV) and decadal trends over the 1986-2005 period.

roland seferian 2/12/15 12:38

Deleted: 8

831 | Figure 19 shows that the transient response of T_{2m} agrees reasonably well with
832 | modern observations (Morice et al., 2012). At the end of the last decades of the
833 | historical simulation (i.e. 1986-2005), CNRM-ESM1 overestimates the T_{2m} increase, a
834 | discrepancy widely shared by other CMIP5 Earth system models (Huber and Knutti,
835 | 2014; Kosaka and Xie, 2013; Meehl et al., 2011; Watanabe et al., 2013). The
836 | amplitude of the simulated recent IAV is in line with the observations (Table 3). In
837 | particular, the model simulates strong cooling followed by stronger warming after the
838 | 1991 mount Pinatubo eruption. Contrasting with temperature, the simulated SIE
839 | poorly agrees with observation-based estimates (Cavalieri et al., 1996; Comiso, 1999;
840 | Rayner et al., 2003). Indeed, CNRM-ESM1 underestimates the mean-state SIE by
841 | about $2 \cdot 10^6 \text{ km}^2$ and overestimates not only the IAV but also the decadal decrease in
842 | extent (Table 3). Therefore, in terms of Arctic sea ice, the skill of CNRM-ESM1 is
843 | similar to CNRM-CM5 as detailed in Massonnet et al. (2012). A better agreement is
844 | found for OHC for which CNRM-ESM1 results agree with observation-based
845 | estimates in term of mean-state and decadal trends (Figure 19, Table 3). Only the
846 | recent IAV in OHC is underestimated by the model, but this latter is poorly
847 | constrained by the observations in regards of the little amount of data available below
848 | 1000 m (Levitus et al., 2012; 2009; Willis et al., 2004).

roland seferian 2/12/15 12:38

Deleted: 8

roland seferian 20/2/16 17:30

Deleted: following

849 | The recent evolution of LCS and OCS agrees with the range of observation-based and
850 | model-derived estimates (Le Quéré et al., 2014; Takahashi et al., 2010) with an uptake
851 | of CO_2 of about 2.1 and 1.7 Pg C y^{-1} for land and ocean, respectively (Table 3).
852 | Underestimation in mean-state OCS is essentially due to the stronger river-induced
853 | offshore outgasing of CO_2 which is about 0.9 Pg C y^{-1} in the model and assumed to be
854 | of 0.45 Pg C y^{-1} in the observation-derived estimates. Both OCS and LCS IAV are
855 | underestimated in CNRM-ESM1 compared to the estimates. For OCS IAV, this
856 | behavior is found in most ocean biogeochemical models as shown in Wanninkhof et
857 | al. (2013). Indeed, simulated IAV from biogeochemical models substantially contrasts
858 | with the large IAV estimated from atmospheric inversion which also contributes to
859 | the mix of observations and model reconstructions that compose the data (Le Quéré et

roland seferian 2/12/15 12:38

Deleted: 8

860 al., 2014). For the land carbon cycle, underestimated LCS IAV may be related to the
861 under-sensitivity of ISBA to climate variability in contrast with the over-sensitivity to
862 the rising CO₂, a behavior shared with other land surface process-based models (Piao
863 et al., 2013). Note that differences in phase between simulated and estimated LCS
864 were expected since the land sink of carbon is approximated from the difference
865 between atmospheric growth rate, land-use emissions and ocean carbon sink
866 (Friedlingstein et al., 2010).

867

868 **5- Summary & conclusions**

869 In this manuscript, we evaluate the ability of the Centre National de Recherches
870 Météorologiques Earth system model version 1 (CNRM-ESM1) to reproduce the
871 modern carbon cycle and its prominent physical drivers. CNRM-ESM1 derives from
872 the atmosphere-ocean general circulation model CNRM-CM5 (Voldoire et al., 2013)
873 that has contributed to CMIP5 and to the fifth IPCC assessment report. This model
874 employs the same resolution and components as CNRM-CM5 although it uses
875 updated versions of the atmospheric model (ARPEGE-CLIMAT v6.1), surface
876 scheme (SURFEXv7.3) and sea-ice model (GELATO6) in addition to a 6-hour
877 coupling frequency. Several biophysical coupling processes are enabled in CNRM-
878 ESM1 thanks to the terrestrial carbon cycle module ISBA (Gibelin et al., 2008) and
879 the marine biogeochemistry module PISCES (Aumont and Bopp, 2006). They consist
880 of the land biosphere-mediated evapotranspiration feedback and the ocean biota heat-
881 trapping feedbacks.

882 Since an earlier version of CNRM-CM5 including the marine biogeochemistry
883 module PISCES was distributed and used in several studies (Frölicher et al., 2014;
884 Laufkötter et al., 2015; Schwinger et al., 2014; Séférian et al., 2013), the inclusion of
885 the terrestrial carbon cycle module ISBA constitutes the major advancement in the
886 CNRM-ESM1 development. Although the ISBA terrestrial carbon cycle module was
887 developed at CNRM in the 2000s, it had never been coupled to an atmosphere-ocean
888 model and run for long climate simulations. Here, we show that ISBA embedded in
889 CNRM-ESM1 reproduces the general pattern of the vegetation and soil carbon stock
890 over the last decades. Although the photosynthesis scheme in ISBA differs from the

891 other state-of-the-art process-based models (e.g., Dalmonech et al., 2014), the model
892 displays similar behavior. That is, it overestimates both the land-vegetation gross
893 primary productivity and the terrestrial ecosystem respiration. The compensation
894 between these two fluxes leads to a correct land carbon sink over the modern period
895 that agrees with the most up-to-date estimates (Friedlingstein et al., 2010; Jung et al.,
896 2011; Le Quéré et al., 2014). The largest model-data mismatch is found in the Tropics
897 where the gross uptake of CO₂ from the vegetation is strongly compensated by an
898 overestimated autotrophic respiration. Maybe apart from this compensating
899 mechanism, our analysis demonstrates that the terrestrial carbon cycle module of
900 CNRM-ESM1 displays similar performances as other IPCC-Class vegetation models
901 (Figures 20 and Figures S11 and S12, see also details in Anav et al. (2013a) and Piao
902 et al. (2013)). The future effort in development will be oriented towards a better
903 parameterization of the carbon absorption and respiration by the vegetation in
904 association with a better representation of ecophysiological processes as detailed in
905 Joetzjer et al. (2015). Further processes like fire-induced disturbance, mortality or
906 linked with permafrost will also be included in order to improve the representation of
907 the live biomass and soil carbon pool.

roland seferian 20/2/16 17:33

Deleted: discrepancies similar to

roland seferian 23/10/15 19:33

Deleted: supplementary materials

908 Regarding the marine biogeochemistry component, CNRM-ESM1 produces results in
909 terms of biogeochemical variables that are comparable to other IPCC-class ocean
910 biogeochemical models (Figure 20). The global distribution of biogeochemical tracers
911 such as oxygen, nutrients and carbon-related fields has been improved with respect to
912 an earlier model version presented in Sférian et al. (2013) (Figure 14 and Figure S9).
913 This change is attributed to a stronger northward flow of deep water masses from the
914 Southern ocean which improves the vertical distribution of biogeochemical tracers.
915 However, the strengthening of the meridional flow of deep water masses has also
916 distorted the vertical structure of some carbon-related fields. Indeed, the unrealistic
917 flow of North Atlantic deep water of about 26.1 Sv tends to deplete the stock of
918 anthropogenic carbon storage between surface and 1200 m (Figure 16c) and
919 consequently to increase it at depth. Since biases in anthropogenic carbon storage
920 compensate across the water column, the simulated anthropogenic carbon storage
921 agrees with 1994 observation-based estimates. Regarding the ocean carbon sink,
922 CNRM-ESM1 simulates a global ocean carbon sink that falls within the lower range
923 of the combination of observation and model estimates over the recent years (Le

roland seferian 20/2/16 19:25

Deleted: t

roland seferian 20/2/16 19:25

Deleted: (

roland seferian 20/2/16 19:25

Deleted: .

roland seferian 27/11/15 16:10

Deleted: improved water conservation in the ocean-sea ice model as well as a higher coupling frequency that induces

roland seferian 20/2/16 17:57

Deleted: While

roland seferian 20/2/16 17:58

Deleted:

roland seferian 20/2/16 18:00

Deleted: .

924 Quéré et al., 2014). This slightly underestimated carbon sink is attributed to larger
925 outgasing of natural CO₂ induced by the riverine input, which fits the upper range of
926 values documented in the fifth IPCC assessment report (IPCC, 2013). Future
927 development will target a better representation of this flux of carbon in close
928 relationship with the recent development on the land surface hydrology (Decharme et
929 al., 2013).

930 We show that CNRM-ESM1 displays results comparable to those of CNRM-CM5 in
931 spite of the inclusion of the global carbon cycle and various biophysical feedbacks.
932 Simulated near-surface temperature, precipitation, incoming shortwave radiation over
933 continents as well as temperature, salinity and mixed-layer depth over oceans broadly
934 agree with observations or satellite-derived product. Except for the salinity and the
935 mixed-layer depth, CNRM-ESM1 display quite similar skill at simulating physical
936 drivers of the global carbon cycle compared to CNRM-CM5. Such a comparison
937 demonstrates the reliability of this model to produce suitable simulations for future
938 climate change projection and impacts studies.

939 In addition to preindustrial control and historical simulations discussed in this
940 manuscript, several other simulations were performed with CNRM-ESM1 following
941 both the CMIP5 and GeoMIP experimental design. The CNRM-ESM1 model outputs
942 (referred as “CNRM-ESM1”) are available for download on ESGF under CMIP5 and
943 GeoMIP projects.

944

945 **Code availability:**

946 A number of model codes developed at CNRM, or in collaboration with CNRM
947 scientists, is available as Open Source code (see [https://opensource.cnrm-game-](https://opensource.cnrm-game-meteo.fr/)
948 [meteo.fr/](http://www.nemo-ocean.eu/) and <http://www.nemo-ocean.eu/>). However, this is not the case for the Earth
949 system model presented in this paper. Part of its code is nevertheless available upon
950 request from the authors of the paper.

951

952 *Acknowledgement:*

953 | *We thank the two anonymous reviewers for their constructive comments and*
954 | *suggestions of the discussion paper.* *This work was supported by Météo-France,*
955 | *CNRS and CERFACS. We particularly acknowledge the support of the team in charge*
956 | *of the CNRM-CM climate model. Supercomputing time was provided by the Météo-*
957 | *France/DSI supercomputing center. Data are published thanks to the ESGF and IS-*
958 | *ENES2 projects. Finally, we are grateful to C. Frauen for her kind advices on the*
959 | *nuances of the English language.*

960 **References:**

- 961 Adler, R. F., Huffman, G. J., Chang, A., Ferraro, R., Xie, P.-P., Janowiak, J., Rudolf,
962 B., Schneider, U., Curtis, S., Bolvin, D., Gruber, A., Susskind, J., Arkin, P. and
963 Nelkin, E.: The Version-2 Global Precipitation Climatology Project (GPCP) Monthly
964 Precipitation Analysis (1979–Present), JOURNAL OF HYDROMETEOROLOGY,
965 4(6), 1147–1167, doi:10.1175/1525-7541(2003)004<1147:TVGPCP>2.0.CO;2, 2003.
- 966 Ammann, C. M., Joos, F., Schimel, D. S., Otto-Bliesner, B. L. and Tomas, R. A.:
967 Solar influence on climate during the past millennium: Results from transient
968 simulations with the NCAR Climate System Model, Proceedings of the National
969 Academy of Sciences, 104(10), 3713–3718, doi:10.1073/pnas.0605064103, 2007.
- 970 | Anav, A., Friedlingstein, P., Kidston, M., Bopp, L., Ciais, P., Cox, P., Jones, C., Jung,
971 M., Myneni, R. and Zhu, Z.: Evaluating the Land and Ocean Components of the
972 Global Carbon Cycle in the CMIP5 Earth System Models, J. Climate, 26(18), 6801–
973 6843, doi:10.1175/JCLI-D-12-00417.1, 2013a.
- 974 Anav, A., Murray-Tortarolo, G., Friedlingstein, P., Sitch, S., Piao, S. and Zhu, Z.:
975 Evaluation of Land Surface Models in Reproducing Satellite Derived Leaf Area Index
976 over the High-Latitude Northern Hemisphere. Part II: Earth System Models, Remote
977 Sensing, 5(8), 3637–3661, doi:10.3390/rs5083637, 2013b.
- 978 Antonov, J. I., Locarnini, R., Boyer, T., Mishonov, A., Garcia, H. and Levitus, S.:
979 World Ocean Atlas 2005 Volume 2: Salinity, NOAA Atlas NESDIS, 62(2), 2006.
- 980 Arora, V. K., Boer, G. J., Friedlingstein, P., Eby, M., Jones, C. D., Christian, J. R.,
981 Bonan, G., Bopp, L., Brovkin, V., Cadule, P., Hajima, T., Ilyina, T., Lindsay, K.,
982 Tjiputra, J. F. and Wu, T.: Carbon–Concentration and Carbon–Climate Feedbacks in
983 CMIP5 Earth System Models, J. Climate, 26(15), 5289–5314, doi:10.1175/JCLI-D-
984 12-00494.1, 2013.
- 985 Aumont, O. and Bopp, L.: Globalizing results from ocean in situ iron fertilization
986 studies, Global Biogeochem. Cycles, 20(2), GB2017, doi:10.1029/2005GB002591,
987 2006.
- 988 Aumont, O., Maier-Reimer, E., Blain, S. and Monfray, P.: An ecosystem model of the
989 global ocean including Fe, Si, P colimitations, Global Biogeochem. Cycles, 17(2),
990 1060, doi:10.1029/2001GB001745, 2003.

roland seferian 10/12/15 19:55

Deleted: Ammann, C. M., Meehl, G. A., Washington, W. M. and Zender, C. S.: A monthly and latitudinally varying volcanic forcing dataset in simulations of 20th century climate, Geophys. Res. Lett., 30(12), 1657, doi:10.1029/2003GL016875, 2003. -

- 991 Axell, L.: Wind-driven internal waves and Langmuir circulations in a numerical ocean
992 model of the southern Baltic Sea, *Journal of Geophysical Research-Oceans*, 107, –,
993 doi:10.1029/2001JC000922, 2002.
- 994 Barnier, B., Madec, G., Penduff, T., Molines, J.-M., Treguier, A.-M., Sommer, J.,
995 Beckmann, A., Biastoch, A., Böning, C., Dengg, J., Derval, C., Durand, E., Gulev, S.,
996 Remy, E., Talandier, C., Theetten, S., Maltrud, M., McClean, J. and Cuevas, B.:
997 Impact of partial steps and momentum advection schemes in a global ocean
998 circulation model at eddy-permitting resolution, *Ocean Dynamics*, 56(5-6), 543–567,
999 doi:10.1007/s10236-006-0082-1, 2006.
- 1000 Battin, T. J., Luysaert, S., Kaplan, L. A., Aufdenkampe, A. K., Richter, A. and
1001 Tranvik, L. J.: The boundless carbon cycle, *Nature Geosci*, 2(9), 598–600,
1002 doi:doi:10.1038/ngeo618, 2009.
- 1003 Blanke, B. and Delecluse, P.: Variability of the Tropical Atlantic Ocean Simulated by
1004 a General Circulation Model with Two Different Mixed-Layer Physics, *J. Phys.*
1005 *Oceanogr.*, 23(7), 1363–1388, doi:10.1175/1520-
1006 0485(1993)023<1363:VOTTAO>2.0.CO;2, 1993.
- 1007 Boone, A., Calvet, J.-C. and Noilhan, J.: Inclusion of a Third Soil Layer in a Land
1008 Surface Scheme Using the Force–Restore Method, *J. Appl. Meteor.*, 38(11), 1611–
1009 1630, doi:10.1175/1520-0450(1999)038<1611:IOATSL>2.0.CO;2, 1999.
- 1010 Bouillon, S., Morales Maqueda, M. Á., Legat, V. and Fichefet, T.: An elastic–
1011 viscous–plastic sea ice model formulated on Arakawa B and C grids, *Ocean*
1012 *Modelling*, 27(3–4), 174–184, 2009.
- 1013 Bretherton, F. P.: Earth system science and remote sensing, *Proc. IEEE*, 73(6), 1118–
1014 1127, doi:10.1109/PROC.1985.13242, 1985.
- 1015 Calvet, J.-C.: Investigating soil and atmospheric plant water stress using physiological
1016 and micrometeorological data, *Agricultural and Forest Meteorology*, 103(3), 229–247,
1017 2000.
- 1018 Calvet, J.-C. and Soussana, J.-F.: Modelling CO₂-enrichment effects using an
1019 interactive vegetation SVAT scheme, *Agricultural and Forest Meteorology*, 108(2),
1020 129–152, doi:10.1016/S0168-1923(01)00235-0, 2001.
- 1021 Calvet, J.-C., Gibelin, A. L., Roujean, J. L., Martin, E., Le Moigne, P., Douville, H.
1022 and Noilhan, J.: Past and future scenarios of the effect of carbon dioxide on plant
1023 growth and transpiration for three vegetation types of southwestern France, *Atmos.*
1024 *Chem. Phys.*, 8(2), 397–406, 2008.
- 1025 Calvet, J.-C., Noilhan, J., Roujean, J.-L., Bessemoulin, P., Cabelguenne, M., Olioso,
1026 A. and Wigneron, J.-P.: An interactive vegetation SVAT model tested against data
1027 from six contrasting sites, *Agricultural and Forest Meteorology*, 92(2), 73–95,
1028 doi:10.1016/S0168-1923(98)00091-4, 1998.
- 1029 Calvet, J.-C., Rivalland, V., Picon-Cochard, C. and Guehl, J.-M.: Modelling forest
1030 transpiration and CO₂ fluxes—response to soil moisture stress, *Agricultural and*

- 1031 Forest Meteorology, 124(3–4), 143–156, 2004.
- 1032 Cariolle, D. and Brard, D.: The Distribution of Ozone and Active Stratospheric
1033 Species: Results of a Two-Dimensional Atmospheric Model, in Atmospheric Ozone,
1034 edited by C. S. Zerefos and A. Ghazi, pp. 77–81, Springer Netherlands. 1985.
- 1035 Cariolle, D. and Teyssevre, H.: A revised linear ozone photochemistry
1036 parameterization for use in transport and general circulation models: multi-annual
1037 simulations, *Atmos. Chem. Phys.*, 7(9), 2183–2196, 2007.
- 1038 Carrer, D., Ceamanos, X. and Roujean, J. L.: Analysis of snow-free vegetation and
1039 bare soil albedos and application to numerical weather prediction, pp. 3789–3792.
1040 2013a.
- 1041 Carrer, D., Roujean, J. L., Lafont, S., Calvet, J.-C., Boone, A., Decharme, B., Delire,
1042 C. and Gastellu-Etchegorry, J. P.: A canopy radiative transfer scheme with explicit
1043 FAPAR for the interactive vegetation model ISBA-A-gs: Impact on carbon fluxes, *J.*
1044 *Geophys. Res. Biogeosci.*, 118(2), 888–903, doi:10.1002/jgrg.20070, 2013b.
- 1045 Cavaliere, D. J., Parkinson, C. L., Gloersen, P. and Zwally, H.: Sea Ice Concentrations
1046 from Nimbus-7 SMMR and DMSP SSM/I-SSMIS Passive Microwave Data, years
1047 1978–2014, Boulder, Colorado USA: NASA DAAC at the National Snow and Ice
1048 Data Center, 1996.
- 1049 Collatz, G. J., Ribas-Carbo, M. and Berry, J. A.: Coupled Photosynthesis-Stomatal
1050 Conductance Model for Leaves of C₄ Plants, *Functional Plant Biol.*, 19(5), 519–538,
1051 1992.
- 1052 Comiso, J. C.: Bootstrap Sea Ice Concentrations from Nimbus-7 SMMR and DMSP
1053 SSM/I-SSMIS (Version 2), 2nd ed., Boulder, Colorado USA: National Snow and Ice
1054 Data Center., 1999.
- 1055 Cox, P., Betts, R., Jones, C., Spall, S. and Totterdell, I.: Acceleration of global
1056 warming due to carbon-cycle feedbacks in a coupled climate model, *Nature*,
1057 408(6809), 184–187, 2000.
- 1058 Dalmonech, D., Foley, A. M., Anav, A., Friedlingstein, P., Friend, A. D., Kidston, M.,
1059 Willeit, M. and Zaehle, S.: Challenges and opportunities to reduce uncertainty in
1060 projections of future atmospheric CO₂: a combined marine and terrestrial biosphere
1061 perspective, *Biogeosciences Discuss.*, 11(2), 2083–2153, doi:10.5194/bgd-11-2083-
1062 2014, 2014.
- 1063 de Baar, H. J. W. and de Jong, J. T. M.: The biogeochemistry of iron in seawater,
1064 edited by D. R. Turner and K. A. Hunter, John Wiley, Hoboken, N. J., 2001.
- 1065 de Lavergne, C., Palter, J. B., Galbraith, E. D., Bernardello, R. and Marinov, I.:
1066 Cessation of deep convection in the open Southern Ocean under anthropogenic
1067 climate change, *Nature Clim. Change*, 4(4), 278–282, doi:10.1038/nclimate2132,
1068 2014.
- 1069 Decharme, B., Martin, E. and Faroux, S.: Reconciling soil thermal and hydrological

- 1070 lower boundary conditions in land surface models, *J Geophys Res-Atmos*, 118(14),
1071 7819–7834, doi:10.1002/jgrd.50631, 2013.
- 1072 DeFries, R. S., Field, C. B., Fung, I., Collatz, G. J. and Bounoua, L.: Combining
1073 satellite data and biogeochemical models to estimate global effects of human-induced
1074 land cover change on carbon emissions and primary productivity, *Global*
1075 *Biogeochem. Cycles*, 13(3), 803–815, doi:10.1029/1999GB900037, 1999.
- 1076 Douville, H., Royer, J. F. and Mahfouf, J. F.: A new snow parameterization for the
1077 Météo-France climate model, *Clim Dyn*, 12(1), 21–35–35, doi:10.1007/BF00208760,
1078 1995.
- 1079 Eppley, R. W., Rogers, J. N. and McCarthy, J. J.: Half-Saturation Constants for
1080 Uptake of Nitrate and Ammonium by Marine Phytoplankton,, 14, 912–920, 1969.
- 1081 Eyring, V., Arblaster, J. M. and Cionni, I.: Long-term ozone changes and associated
1082 climate impacts in CMIP5 simulations - Eyring - 2013 - *Journal of Geophysical*
1083 *Research: Atmospheres* - Wiley Online Library, *Journal of Climate*, 2013.
- 1084 Fairall, C. W., Bradley, E. F., Hare, J. E., Grachev, A. A. and Edson, J. B.: Bulk
1085 Parameterization of Air–Sea Fluxes: Updates and Verification for the COARE
1086 Algorithm, *J. Climate*, 16(4), 571–591, doi:10.1175/1520-
1087 0442(2003)016<0571:BPOASF>2.0.CO;2, 2003.
- 1088 Farquhar, G. D., Caemmerer, S. and Berry, J. A.: A biochemical model of
1089 photosynthetic CO₂ assimilation in leaves of C₃ species, *Planta*, 149(1), 78–90,
1090 doi:10.1007/BF00386231, 1980.
- 1091 Fetterer, F., Knowles, K., Meier, W. and Savoie, M.: *Sea Ice Index*, 2014 ed.,
1092 Boulder, Colorado USA: National Snow and Ice Data Center. [online] Available
1093 from: <http://dx.doi.org/10.7265/N5QJ7F7W>, 2002.
- 1094 [Flato, G. M.: Earth system models: an overview. *WIREs Clim Change*. 2\(6\). 783–](#)
1095 [800. doi:10.1002/wcc.148, 2011.](#)
- 1096 Friedlingstein, P. and Prentice, I. C.: Carbon-climate feedbacks: a review of model
1097 and observation based estimates, *Curr Opin Env Sust*, 2(4), 251–257,
1098 doi:10.1016/j.cosust.2010.06.002, 2010.
- 1099 Friedlingstein, P., Houghton, R. A., Marland, G., Hackler, J., Boden, T. A., Conway,
1100 T. J., Canadell, J. G., Raupach, M. R., Ciais, P. and Le Quéré, C.:
1101 Friedlignstein_2010.Update of CO₂ emissions.Naturegeo, Nature Publishing Group,
1102 3(12), 811–812, doi:10.1038/ngeo1022, 2010.
- 1103 Friedlingstein, P., Meinshausen, M., Arora, V. K., Jones, C. D., Anav, A., Liddicoat,
1104 S. K. and Knutti, R.: Uncertainties in CMIP5 climate projections due to carbon cycle
1105 feedbacks, *J. Climate*, 130917124100006, doi:doi: 10.1175/JCLI-D-12-00579.1,
1106 2013.
- 1107 Frölicher, T. L., Sarmiento, J. L., Paynter, D. J., Dunne, J. P., Krasting, J. P. and
1108 Winton, M.: Dominance of the Southern Ocean in anthropogenic carbon and heat

roland seferian 20/2/16 17:05

Formatted: Font:12 pt

roland seferian 20/2/16 17:05

Formatted: Don't adjust space between Asian text and numbers

roland seferian 20/2/16 17:05

Formatted: French

- 1109 uptake in CMIP5 models, *J. Climate*, 141031131835005, doi:10.1175/JCLI-D-14-
1110 00117.1, 2014.
- 1111 Geider, R., MacIntyre, H. and Kana, T.: A dynamic regulatory model of
1112 phytoplanktonic acclimation to light, nutrients, and temperature, *Limnology and*
1113 *Oceanography*, 43(4), 679–694, 1998.
- 1114 Gibelin, A.-L., Calvet, J.-C. and Viovy, N.: Modelling energy and CO2 fluxes with an
1115 interactive vegetation land surface model-Evaluation at high and middle latitudes,
1116 *Agricultural and Forest Meteorology*, 148(10), 1611–1628,
1117 doi:10.1016/j.agrformet.2008.05.013, 2008.
- 1118 Gibelin, A.-L., Calvet, J.-C., Roujean, J.-L., Jarlan, L. and Los, S. O.: Ability of the
1119 land surface model ISBA-A-gs to simulate leaf area index at the global scale:
1120 Comparison with satellites products, *J. Geophys. Res.*, 111(D18), D18102–,
1121 doi:10.1029/2005JD006691, 2006.
- 1122 Goudriaan, J., van Laar, H. H., van Keulen, H. and Louwse, W.: Photosynthesis,
1123 CO2 and Plant Production, in *NATO ASI Science*, vol. 86, edited by W. Day and R.
1124 K. Atkin, pp. 107–122–122, Springer US, Boston, MA. 1985.
- 1125 Hajima, T., Kawamiya, M., Watanabe, M., Kato, E., Tachiiri, K., Sugiyama, M.,
1126 Watanabe, S., Okajima, H. and Ito, A.: Modeling in Earth system science up to and
1127 beyond IPCC AR5, *Progress in Earth and Planetary Science*, 1(1), 29–25,
1128 doi:10.1186/s40645-014-0029-y, 2014.
- 1129 Harris, I., Jones, P. D., Osborn, T. J. and Lister, D. H.: Updated high-resolution grids
1130 of monthly climatic observations - the CRU TS3.10 Dataset, *Int. J. Climatol.*, 34(3),
1131 623–642, doi:10.1002/joc.3711, 2013.
- 1132 Heuzé, C., Heywood, K. J., Stevens, D. P. and Ridley, J. K.: Southern Ocean bottom
1133 water characteristics in CMIP5 models, *Geophys. Res. Lett.*, n/a–n/a,
1134 doi:10.1002/grl.50287, 2013.
- 1135 Houghton, R. A.: Balancing the Global Carbon Budget, *Annu. Rev. Earth Planet. Sci.*,
1136 35(1), 313–347, doi:10.1146/annurev.earth.35.031306.140057, 2007.
- 1137 Huber, M. and Knutti, R.: Natural variability, radiative forcing and climate response
1138 in the recent hiatus reconciled, *Nature Geosci*, 7(9), 651–656, doi:10.1038/ngeo2228,
1139 2014.
- 1140 Hunke, E. C. and Dukowicz, J. K.: An Elastic–Viscous–Plastic Model for Sea Ice
1141 Dynamics, *J. Phys. Oceanogr.*, 27(9), 1849–1867, doi:doi: 10.1175/1520-
1142 0485(1997)027<1849:AEVPMF>2.0.CO;2, 1997.
- 1143 IPCC: IPCC, 2007: *Climate Change 2007: The Physical Science Basis*, edited by S.
1144 Solomon, D. Qin, M. Manning, Z. Chen, M. Marquis, K. B. Averyt, M. Tignor, and
1145 H. L. Miller, Cambridge University Press, Cambridge, United Kingdom and New
1146 York, NY, USA. 2007.
- 1147 IPCC: IPCC, 2013: *Climate Change 2013: The Physical Science Basis.*, edited by T.

- 1148 F. Stoker, D. Qin, G. Plattner, M. Tignor, S. K. Allen, J. Boschung, A. Nauels, Y. Xia,
1149 V. Bex, and P. M. Midgley, Cambridge Univ Press, Cambridge, United Kingdom and
1150 New York, NY, USA. 2013.
- 1151 Jacobs, C. M. J., van den Hurk, B. M. M. and de Bruin, H. A. R.: Stomatal behaviour
1152 and photosynthetic rate of unstressed grapevines in semi-arid conditions, *Agricultural*
1153 *and Forest Meteorology*, 80(2–4), 111–134, 1996.
- 1154 Jacobson, A. R., Mikaloff Fletcher, S. E., Gruber, N., Sarmiento, J. L. and Gloor, M.:
1155 A joint atmosphere–ocean inversion for surface fluxes of carbon dioxide: 1. Methods
1156 and global-scale fluxes, *Global Biogeochem. Cycles*, 21(1),
1157 doi:10.1029/2005GB002556, 2007.
- 1158 Jickells, T. and Spokes, L.: *The biogeochemistry of iron in seawater*, edited by D. R.
1159 Turner and K. A. Hunter, John Wiley, Hoboken, N. J., 2001.
- 1160 Joetzjer, E., Delire, C., Douville, H., Ciais, P., Decharme, B., Carrer, D., Verbeeck,
1161 H., De Weirdt, M. and Bonal, D.: Improving the ISBAcc land surface model
1162 simulation of water and carbon fluxes and stocks over the Amazon forest, *Geosci.*
1163 *Model Dev. Discuss.*, 8(2), 1293–1336, 2015.
- 1164 Joetzjer, E., Delire, C., Douville, H., Ciais, P., Decharme, B., Fisher, R.,
1165 Christoffersen, B., Calvet, J.-C., da Costa, A. C. L., Ferreira, L. V. and MEIR, P.:
1166 Predicting the response of the Amazon rainforest to persistent drought conditions
1167 under current and future climates: a major challenge for global land surface models,
1168 *Geosci. Model Dev*, 7(6), 2933–2950, doi:10.5194/gmd-7-2933-2014, 2014.
- 1169 Johns, W. E., Baringer, M. O., Beal, L. M., Cunningham, S. A., Kanzow, T., Bryden,
1170 H. L., Hirschi, J. J. M., Marotzke, J., Meinen, C. S., Shaw, B. and Curry, R.:
1171 Continuous, Array-Based Estimates of Atlantic Ocean Heat Transport at 26.5°N, *J.*
1172 *Climate*, 24(10), 2429–2449, doi:10.1175/2010JCLI3997.1, 2011.
- 1173 Johnson, K., Chavez, F. and Friederich, G.: Continental-shelf sediment as a primary
1174 source of iron for coastal phytoplankton, *Nature*, 398(6729), 697–700, 1999.
- 1175 JRC, F. I. I. I.: *Harmonized World Soil Database (version 1.10)*, edited by F. I. I. I.
1176 JRC, FAO, Rome, Italy and IIASA, Laxenburg, Austria. 2012.
- 1177 Jung, M., Reichstein, M., Margolis, H. A., Cescatti, A., Richardson, A. D., Arain, M.
1178 A., Arneth, A., Bernhofer, C., Bonal, D., Chen, J., Gianelle, D., Gobron, N., Kiely,
1179 G., Kutsch, W., Lasslop, G., Law, B. E., Lindroth, A., Merbold, L., Montagnani, L.,
1180 Moors, E. J., Papale, D., Sottocornola, M., Vaccari, F. and Williams, C.: Global
1181 patterns of land-atmosphere fluxes of carbon dioxide, latent heat, and sensible heat
1182 derived from eddy covariance, satellite, and meteorological observations, *J. Geophys.*
1183 *Res.*, 116(G3), G00J07, doi:10.1029/2010JG001566, 2011.
- 1184 Key, R., Kozyr, A., Sabine, C., Lee, K., Wanninkhof, R., Bullister, J., Feely, R.,
1185 Millero, F., Mordy, C. and Peng, T.: *A global ocean carbon climatology: Results from*
1186 *Global Data Analysis Project (GLODAP)*, *Global Biogeochem. Cycles*, 18(4),
1187 doi:10.1029/2004GB002247, 2004.

- 1188 Khatiwala, S., Tanhua, T., Mikaloff Fletcher, S., Gerber, M., Doney, S. C., Graven, H.
1189 D., Gruber, N., McKinley, G. A., Murata, A., Rios, A. F. and Sabine, C. L.: Global
1190 ocean storage of anthropogenic carbon, *Biogeosciences*, 10(4), 2169–2191,
1191 doi:10.5194/bg-10-2169-2013, 2013.
- 1192 Koch-Larrouy, A., Lengaigne, M., Terray, P., Madec, G. and Masson, S.: Tidal
1193 mixing in the Indonesian Seas and its effect on the tropical climate system, *Climate*
1194 *Dynamics*, 34, 891–904, doi:10.1007/s00382-009-0642-4, 2010.
- 1195 Koch-Larrouy, A., Madec, G., Bouruet-Aubertot, P., Gerkema, T., Bessières, L. and
1196 Molcard, R.: On the transformation of Pacific Water into Indonesian Throughflow
1197 Water by internal tidal mixing, *Geophys. Res. Lett.*, 34(4),
1198 doi:10.1029/2006GL028405, 2007.
- 1199 Kosaka, Y. and Xie, S.-P.: Recent global-warming hiatus tied to equatorial Pacific
1200 surface cooling, *Nature*, 501(7467), 403–407, doi:10.1038/nature12534, 2013.
- 1201 Krinner, G., Viovy, N., de Noblet-Ducoudré, N., Ogée, J., Polcher, J., Friedlingstein,
1202 P., Ciais, P., Sitch, S. and Prentice, I. C.: A dynamic global vegetation model for
1203 studies of the coupled atmosphere-biosphere system, *Global Biogeochem. Cycles*,
1204 19(1), 1–33, 2005.
- 1205 Landschützer, P., Gruber, N., Bakker, D. C. E. and SCHUSTER, U.: Recent
1206 variability of the global ocean carbon sink, *Global Biogeochem. Cycles*,
1207 2014GB004853, doi:10.1002/2014GB004853, 2014.
- 1208 Laufkötter, C., Vogt, M., Gruber, N., Aita-Noguchi, M., Aumont, O., Bopp, L.,
1209 Buitenhuis, E., Doney, S. C., Dunne, J., Hashioka, T., Hauck, J., Hirata, T., John, J.,
1210 Le Quéré, C., Lima, I. D., Nakano, H., Séférian, R., Totterdell, I., Vichi, M. and
1211 Völker, C.: Drivers and uncertainties of future global marine primary production in
1212 marine ecosystem models, *Biogeosciences Discuss.*, 12(4), 3731–3824, 2015.
- 1213 Le Quéré, C., Moriarty, R., Andrew, R. M., Peters, G. P., Ciais, P., Friedlingstein, P.,
1214 Jones, S. D., Sitch, S., Tans, P., Arneeth, A., Boden, T. A., Bopp, L., Bozec, Y.,
1215 Canadell, J. G., Chevallier, F., Cosca, C. E., Harris, I., Hoppema, M., Houghton, R.
1216 A., House, J. I., Jain, A., Johannessen, T., Kato, E., Keeling, R. F., Kitidis, V., Klein
1217 Goldewijk, K., Koven, C., Landa, C. S., Landschützer, P., Lenton, A., Lima, I. D.,
1218 Marland, G., Mathis, J. T., Metz, N., Nojiri, Y., Olsen, A., Ono, T., Peters, W., Pfeil,
1219 B., Poulter, B., Raupach, M. R., Regnier, P., Rödenbeck, C., Saito, S., Salisbury, J. E.,
1220 SCHUSTER, U., Schwinger, J., Séférian, R., Segschneider, J., Steinhoff, T., Stocker,
1221 B. D., Sutton, A. J., Takahashi, T., Tilbrook, B., van der Werf, G. R., Viovy, N.,
1222 Wang, Y. P., Wanninkhof, R., Wiltshire, A. and Zeng, N.: Global carbon budget
1223 2014, *ESSDD*, 7(2), 521–610, 2014.
- 1224 Lengaigne, M., Madec, G., Bopp, L., Menkes, C., Aumont, O. and Cadule, P.: Bio-
1225 physical feedbacks in the Arctic Ocean using an Earth system model, *Geophys. Res.*
1226 *Lett.*, 36(21), L21602–, doi:10.1029/2009GL040145, 2009.
- 1227 Lengaigne, M., Menkes, C., Aumont, O., Gorgues, T., Bopp, L., André, J.-M. and
1228 Madec, G.: Influence of the oceanic biology on the tropical Pacific climate in a
1229 coupled general circulation model, *Climate Dynamics*, 28(5), 503–516,

- 1230 doi:10.1007/s00382-006-0200-2, 2006.
- 1231 Levitus, S., Antonov, J. I., Baranova, O. K., Boyer, T. P., Coleman, C. L., Garcia, H.
1232 E., Grodsky, A. I., Johnson, D. R., Locarnini, R. A., Mishonov, A. V., Reagan, J. R.,
1233 Sazama, C. L., Seidov, D., Smolyar, I., Yarosh, E. S. and Zweng, M. M.: The World
1234 Ocean Database TI , Data Science Journal, 12 IS -, WDS229–WDS234, 2013.
- 1235 Levitus, S., Antonov, J. I., Boyer, T. P., Baranova, O. K., Garcia, H. E., Locarnini, R.
1236 A., Mishonov, A. V., Reagan, J. R., Seidov, D., Yarosh, E. S. and Zweng, M. M.:
1237 World ocean heat content and thermosteric sea level change (0-2000 m), 1955-2010,
1238 Geophys. Res. Lett., 39(10), n/a–n/a, doi:10.1029/2012GL051106, 2012.
- 1239 Levitus, S., Antonov, J. I., Boyer, T. P., Locarnini, R. A., Garcia, H. E. and
1240 Mishonov, A. V.: Global ocean heat content 1955–2008 in light of recently revealed
1241 instrumentation problems, Geophys. Res. Lett., 36(7), doi:10.1029/2008GL037155,
1242 2009.
- 1243 Levitus, S., Conkright, M. E., Reid, J. L., Najjar, R. G. and Mantyla, A.: Distribution
1244 of nitrate, phosphate and silicate in the world oceans, Progress in Oceanography,
1245 31(3), 245–273, 1993.
- 1246 Lipschultz, F., Wofsy, S. C., Ward, B. B., Codispoti, L. A., Friedrich, G. and Elkins,
1247 J. W.: Bacterial transformations of inorganic nitrogen in the oxygen-deficient waters
1248 of the Eastern Tropical South Pacific Ocean, Deep-Sea Res, 37(10), 1513–1541,
1249 doi:doi: 10.1016/0198-0149(90)90060-9, 1990.
- 1250 Locarnini, R. A., Mishonov, A. V., Antonov, J. I., Boyer, T. P., Garcia, H. E.,
1251 Baranova, O. K., Zweng, M. M. and Johnson, D. R.: World Ocean Atlas 2005
1252 Volume 1: Temperature,, 2006.
- 1253 Ludwig, W., Probst, J. and Kempe, S.: Predicting the oceanic input of organic carbon
1254 by continental erosion, Global Biogeochem. Cycles, 10(1), 23–41, 1996.
- 1255 Madec, G.: NEMO ocean engine, Institut Pierre-Simon Laplace (IPSL), France.
1256 Institut Pierre-Simon Laplace (IPSL). [online] Available from: [http://www.nemo-](http://www.nemo-ocean.eu/About-NEMO/Reference-manuals)
1257 [ocean.eu/About-NEMO/Reference-manuals](http://www.nemo-ocean.eu/About-NEMO/Reference-manuals), 2008.
- 1258 Maier-Reimer, E.: Geochemical cycles in an ocean general circulation model.
1259 Preindustrial tracer distributions, Global Biogeochem. Cycles, 7(3), 645,
1260 doi:10.1029/93GB01355, 1993.
- 1261 Majkut, J. D., Sarmiento, J. L. and Rodgers, K. B.: A Growing Oceanic Carbon
1262 Uptake: Results from an inversion study of surface pCO₂ data, Global Biogeochem.
1263 Cycles, 2013GB004585, doi:10.1002/2013GB004585, 2014.
- 1264 Masson, V., Champeaux, J.-L., Chauvin, F., Meriguet, C. and Lacaze, R.: A Global
1265 Database of Land Surface Parameters at 1-km Resolution in Meteorological and
1266 Climate Models, J. Climate, 16(9), 1261–1282, doi:doi: 10.1175/1520-
1267 0442(2003)16<1261:AGDOLS>2.0.CO;2, 2013a.
- 1268 Masson, V., Le Moigne, P., Martin, E., Faroux, S., Alias, A., Alkama, R., Belamari,

- 1269 S., Barbu, A., Boone, A., Bouyssel, F., Brousseau, P., Brun, E., Calvet, J.-C., Carrer,
1270 D., Decharme, B., Delire, C., Donier, S., Essaouini, K., Gibelin, A. L., Giordani, H.,
1271 Habets, F., Jidane, M., Kerdraon, G., Kourzeneva, E., Lafaysse, M., Lafont, S.,
1272 Lebeaupin Brossier, C., Lemonsu, A., Mahfouf, J. F., Marguinaud, P., Mokhtari, M.,
1273 Morin, S., Pigeon, G., Salgado, R., Seity, Y., Taillefer, F., Tanguy, G., Tulet, P.,
1274 Vincendon, B., Vionnet, V. and Voldoire, A.: The SURFEXv7.2 land and ocean
1275 surface platform for coupled or offline simulation of earth surface variables and
1276 fluxes, *Geosci. Model Dev*, 6(4), 929–960, doi:10.5194/gmd-6-929-2013-supplement,
1277 2013b.
- 1278 Massonnet, F., Fichet, T., Goosse, H., Bitz, C. M., Philippon-Berthier, G., Holland,
1279 M. M. and Barriat, P. Y.: Constraining projections of summer Arctic sea ice, *The*
1280 *Cryosphere*, 6(6), 1383–1394, doi:10.5194/tc-6-1383-2012, 2012.
- 1281 Meehl, G. A., Arblaster, J. M., Fasullo, J. T., Hu, A. and Trenberth, K. E.: Model-
1282 based evidence of deep-ocean heat uptake during surface-temperature hiatus periods,
1283 *Nature Climate change*, 1(7), 360–364, doi:10.1038/nclimate1229, 2011.
- 1284 Mellor, G. and Blumberg, A.: Wave Breaking and Ocean Surface Layer Thermal
1285 Response, *J. Phys. Oceanogr.*, 34(3), 693–698, doi:doi: 10.1175/2517.1, 2004.
- 1286 Merryfield, W., Holloway, G. and Gargett, A.: A global ocean model with double-
1287 diffusive mixing, *J. Phys. Oceanogr.*, 29(6), 1124–1142, 1999.
- 1288 Middelburg, J., Soetaert, K., Herman, P. and Heip, C.: Denitrification in marine
1289 sediments: A model study, *Global Biogeochem. Cycles*, 10(4), 661–673, 1996.
- 1290 Mignot, J., Swingedouw, D., Deshayes, J., Marti, O., Talandier, C., Séférian, R.,
1291 Lengaigne, M. and Madec, G.: On the evolution of the oceanic component of the
1292 IPSL climate models from CMIP3 to CMIP5: A mean state comparison, *Ocean*
1293 *Modelling*, (0 SP - EP - PY - T2 -), 2013.
- 1294 Mikaloff Fletcher, S. E., Gruber, N., Jacobson, A. R., Gloor, M., Doney, S. C.,
1295 Dutkiewicz, S., Gerber, M., Follows, M., Joos, F., Lindsay, K., Menemenlis, D.,
1296 Mouchet, A., Müller, S. A. and Sarmiento, J. L.: Inverse estimates of the oceanic
1297 sources and sinks of natural CO₂ and the implied oceanic carbon transport, *Global*
1298 *Biogeochem. Cycles*, 21(1), GB1010, doi:10.1029/2006GB002751, 2007.
- 1299 Monod, J.: *Recherches sur la croissance des cultures bactériennes*, Hermann, Paris.
1300 1942.
- 1301 Moore, J., Doney, S. and Lindsay, K.: Upper ocean ecosystem dynamics and iron
1302 cycling in a global three-dimensional model, *Global Biogeochem. Cycles*, 18(4), –,
1303 doi:10.1029/2004GB002220, 2004.
- 1304 Moore, J., Doney, S., Kleypas, J., Glover, D. and Fung, I.: An intermediate
1305 complexity marine ecosystem model for the global domain, *Deep Sea Research Part*
1306 *II: Topical Studies in Oceanography*, 49, 403–462, 2002.
- 1307 Morel, A.: Optical Modeling of the Upper Ocean in Relation to Its Biogenous Matter
1308 Content (Case-I Waters), *Journal of Geophysical Research-Oceans*, 93, 10749–10768,

- 1309 1988.
- 1310 Morice, C. P., Kennedy, J. J., Rayner, N. A. and Jones, P. D.: Quantifying
1311 uncertainties in global and regional temperature change using an ensemble of
1312 observational estimates: The HadCRUT4 data set, *J. Geophys. Res.*, 117(D8),
1313 D08101, doi:10.1029/2011JD017187, 2012.
- 1314 Noilhan, J. and Planton, S.: A Simple Parameterization of Land Surface Processes for
1315 Meteorological Models, *Monthly Weather Review*, 117(3), 536–549,
1316 doi:10.1175/1520-0493(1989)117<0536:ASPOLS>2.0.CO;2, 1989.
- 1317 O'Reilly, J. E., Maritorena, S., Mitchell, B. G., Siegel, D. A., Carder, K. L., Garver, S.
1318 A., Kahru, M. and McClain, C.: Ocean color chlorophyll algorithms for SeaWiFS, *J.*
1319 *Geophys. Res.*, 103(C11), 24937–24953, doi:10.1029/98JC02160, 1998.
- 1320 Oki, T. and Sud, Y. C.: Design of Total Runoff Integrating Pathways (TRIP)—A
1321 Global River Channel Network, *Earth Interactions*, 2, 1–36, 1997.
- 1322 Orsi, A., Johnson, G. and Bullister, J.: Circulation, mixing, and production of
1323 Antarctic Bottom Water, *Progress in Oceanography*, 1999.
- 1324 Parton, W. J., Stewart, J. W. B. and Cole, C. V.: Dynamics of C, N, P and S in
1325 grassland soils: a model, *Biogeochemistry*, 5(1), 109–131, doi:10.1007/BF02180320,
1326 1988.
- 1327 Pérez, F. F., Mercier, H., Vázquez-Rodríguez, M., Lherminier, P., Velo, A., Pardo, P.
1328 C., Rosón, G. and Ríos, A. F.: Atlantic Ocean CO₂ uptake reduced by weakening of
1329 the meridional overturning circulation, *Nature Geosci.*, 6(2), 146–152,
1330 doi:10.1038/ngeo1680, 2013.
- 1331 Piao, S., Sitch, S., Ciais, P., Friedlingstein, P., Peylin, P., Wang, X., Ahlström, A.,
1332 Anav, A., Canadell, J. G., Cong, N., Huntingford, C., Jung, M., Levis, S., Levy, P. E.,
1333 Li, J., Lin, X., Lomas, M. R., Lu, M., Luo, Y., Ma, Y., Myneni, R. B., Poulter, B.,
1334 Sun, Z., Wang, T., Viovy, N., Zaehle, S. and Zeng, N.: Evaluation of terrestrial carbon
1335 cycle models for their response to climate variability and to CO₂ trends, *Global*
1336 *Change Biol.*, 19(7), 2117–2132, doi:10.1111/gcb.12187, 2013.
- 1337 Pinker, R. T. and Laszlo, I.: Modeling Surface Solar Irradiance for Satellite
1338 Applications on a Global Scale, *J. Appl. Meteor.*, 31(2), 194–211, doi:10.1175/1520-
1339 0450(1992)031<0194:MSSIFS>2.0.CO;2, 1992.
- 1340 Rawlins, M. A., McGuire, A. D., Kimball, J. K., Dass, P., Lawrence, D., Burke, E.,
1341 Chen, X., Delire, C., Koven, C., MacDougall, A., Peng, S., Rinke, A., Saito, K.,
1342 Zhang, W., Alkama, R., J Bohn, T., Ciais, P., Decharme, B., Gouttevin, I., Hajima, T.,
1343 Ji, D., Krinner, G., Lettenmaier, D. P., Miller, P., Moore, J. C., Smith, B. and
1344 Sueyoshi, T.: Assessment of model estimates of land–atmosphere CO₂ exchange
1345 across Northern Eurasia, *Biogeosciences Discuss.*, 12(3), 2257–2305,
1346 doi:10.5194/bgd-12-2257-2015, 2015.
- 1347 Rayner, N. A., Parker, D. E., Horton, E. B., Folland, C. K., Alexander, L. V., Rowell,
1348 D. P., Kent, E. C. and Kaplan, A.: Global analyses of sea surface temperature, sea ice,

- 1349 and night marine air temperature since the late nineteenth century, *J. Geophys. Res.*,
1350 108(D14), 4407, 2003.
- 1351 Regnier, P., Friedlingstein, P., Ciais, P., Mackenzie, F. T., Gruber, N., Janssens, I. A.,
1352 Laruelle, G. G., Lauerwald, R., Luyssaert, S., Andersson, A. J., Arndt, S., Arnosti, C.,
1353 Borges, A. V., Dale, A. W., Gallego-Sala, A., Godderis, Y., Goossens, N., Hartmann,
1354 J., Heinze, C., Ilyina, T., Joos, F., LaRowe, D. E., Leifeld, J., Meysman, F. J. R.,
1355 Munhoven, G., Raymond, P. A., Spahni, R., Suntharalingam, P. and Thullner, M.:
1356 Anthropogenic perturbation of the carbon fluxes from land to ocean, *Nature Geosci*,
1357 advance online publication SP - EP -(8), 597–607, doi:10.1038/ngeo1830, 2013.
- 1358 Running, S. W., Nemani, R. R., Heinsch, F. A., Zhao, M., Reeves, M. and Hashimoto,
1359 H.: A Continuous Satellite-Derived Measure of Global Terrestrial Primary
1360 Production, *BioScience*, 54(6), 547–560 [online] Available from:
1361 <http://bioscience.oxfordjournals.org/content/54/6/547.abstract>, 2004.
- 1362 Sabine, C., Feely, R., Gruber, N., Key, R., Lee, K., Bullister, J., Wanninkhof, R.,
1363 Wong, C., Wallace, D., Tilbrook, B., Millero, F., Peng, T., Kozyr, A., Ono, T. and
1364 Rios, A.: The oceanic sink for anthropogenic CO₂, *Science*, 305(5682), 367–371,
1365 doi:{10.1126/science.1097403}, 2004.
- 1366 Salas y Mélia, D.: A global coupled sea ice–ocean model, *Ocean Modelling*, 4(2),
1367 137–172, doi:doi: 10.1016/S1463-5003(01)00015-4, 2002.
- 1368 Sallée, J. B., Shuckburgh, E., Bruneau, N., Meijers, A. J. S., Bracegirdle, T. J., Wang,
1369 Z. and Roy, T.: Assessment of Southern Ocean water mass circulation and
1370 characteristics in CMIP5 models: Historical bias and forcing response, *Journal of*
1371 *Geophysical Research-Oceans*, 118(4), 1830–1844, doi:10.1002/jgrc.20135, 2013.
- 1372 Sallée, J., Speer, K. and Rintoul, S. R.: Zonally asymmetric response of the Southern
1373 Ocean mixed-layer depth to the Southern Annular Mode, *Nature Geosci*, 3(4), 273–
1374 279, doi:10.1038/ngeo812, 2010.
- 1375 Sallée, J.-B., Matear, R. J., Rintoul, S. R. and Lenton, A.: Localized subduction of
1376 anthropogenic carbon dioxide in the Southern Hemisphere oceans, *Nature Geosci*,
1377 5(8), 579–584, doi:10.1038/ngeo1523, 2012.
- 1378 Sander, S. P., Golden, D. M., Kurylo, M. J. and Moortgat, G. K.: BEACON eSpace at
1379 Jet Propulsion Laboratory: Chemical kinetics and photochemical data for use in
1380 Atmospheric Studies Evaluation Number 15., 2006.
- 1381 Sarmiento, J. L. and Gruber, N.: *Ocean Biogeochemical Dynamics*, Princeton
1382 University Press. 2006.
- 1383 Sarrat, C., Noilhan, J., Dolman, A. J., Gerbig, C., Ahmadov, R., Tolk, L. F., Meesters,
1384 A. G. C. A., Hutjes, R. W. A., Maat, Ter, H. W., Pérez-Landa, G. and Donier, S.:
1385 Atmospheric CO₂ modeling at the regional scale: an intercomparison of 5 meso-scale
1386 atmospheric models, *Biogeosciences*, 4(6), 1115–1126, 2007.
- 1387 Schwinger, J., Tjiputra, J. F., Heinze, C., Bopp, L., Christian, J. R., Gehlen, M.,
1388 Ilyina, T., Jones, C. D., Salas-Mélia, D., Segsneider, J., Séférian, R. and Totterdell,

- 1389 I.: Non-linearity of ocean carbon cycle feedbacks in CMIP5 earth system models, J.
1390 Climate, 27(11), 140310121516000, doi:10.1175/JCLI-D-13-00452.1, 2014.
- 1391 S  ferian, R., Bopp, L., Gehlen, M., Orr, J., Eth  , C., Cadule, P., Aumont, O., Salas y
1392 M  lia, D., Voldoire, A. and Madec, G.: Skill assessment of three earth system models
1393 with common marine biogeochemistry, Climate Dynamics, 40(9-10), 2549–2573,
1394 doi:10.1007/s00382-012-1362-8, 2013.
- 1395 S  ferian, R., Ribes, A. and Bopp, L.: Detecting the anthropogenic influences on recent
1396 changes in ocean carbon uptake, Geophys. Res. Lett., 2014GL061223,
1397 doi:10.1002/2014GL061223, 2014.
- 1398 [Sheffield, J., Goteti, G. and Wood, E. F.: Development of a 50-Year High-Resolution](#)
1399 [Global Dataset of Meteorological Forcings for Land Surface Modeling, J. Climate,](#)
1400 [19\(13\), 3088–3111, doi:10.1175/JCLI3790.1, 2006.](#)
- 1401 Simmons, H., Jayne, S., St Laurent, L. and Weaver, A.: Tidally driven mixing in a
1402 numerical model of the ocean general circulation, Ocean Modelling, 6, 245–263,
1403 doi:10.1016/S1463-5003(03)00011-8, 2004.
- 1404 Soetaert, K., Middelburg, J., Herman, P. and Buis, K.: On the coupling of benthic and
1405 pelagic biogeochemical models, Earth-Sci Rev, 51, 173–201, 2000.
- 1406 Sunda, W. and Huntsman, S.: Interrelated influence of iron, light and cell size on
1407 marine phytoplankton growth, Nature, 390(6658), 389–392, 1997.
- 1408 Szczypta, C., Calvet, J.-C., Maignan, F., Dorigo, W., Baret, F. and Ciais, P.:
1409 Suitability of modelled and remotely sensed essential climate variables for monitoring
1410 Euro-Mediterranean droughts, Geosci. Model Dev, 7(3), 931–946, 2014.
- 1411 Szczypta, C., Decharme, B., Carrer, D., Calvet, J.-C., Lafont, S., Somot, S., Faroux, S.
1412 and Martin, E.: Impact of precipitation and land biophysical variables on the
1413 simulated discharge of European and Mediterranean rivers, HESS, 16(9), 3351–3370,
1414 2012.
- 1415 Szopa, S., Balkanski, Y., Schulz, M., Bekki, S., Cugnet, D., Fortems-Cheiney, A.,
1416 Turquety, S., Cozic, A., D  andreis, C., Hauglustaine, D., Idelkadi, A., Lath  re, J.,
1417 Lef  vre, F., Marchand, M., Vuolo, R., Yan, N. and Dufresne, J.-L.: Aerosol and ozone
1418 changes as forcing for climate evolution between 1850 and 2100, Climate Dynamics,
1419 40(9-10), 2223–2250, doi:10.1007/s00382-012-1408-y, 2013.
- 1420 Takahashi, T.: Climatological mean and decadal change in surface ocean pCO₂, and
1421 net sea–air CO₂ flux over the global oceans, Deep Sea Research Part II: Topical
1422 Studies in Oceanography, 56(8-10), 554–577, doi:10.1016/j.dsr2.2008.12.009, 2009.
- 1423 Takahashi, T., Broecker, W. and Langer, S.: Redfield Ratio Based on Chemical-Data
1424 From Isopycnal Surfaces, Journal of Geophysical Research-Oceans, 90, 6907–6924,
1425 1985.
- 1426 Takahashi, T., Sutherland, S. C. and Kozyr, A.: Global Ocean Surface Water Partial
1427 Pressure of CO₂ Database: Measurements Performed during 1968–2010 (Version

roland seferian 10/12/15 19:56

Formatted: Font:12 pt

roland seferian 10/12/15 19:56

Deleted: -

- 1428 2010), edited by O. CDIAC-152, CDIAC-152, ORNL. 2010.
- 1429 Talley, L. D., Reid, J. L. and Robbins, P. E.: Data-Based Meridional Overturning
1430 Streamfunctions for the Global Ocean, *J. Climate*, 16(19), 3213–3226,
1431 doi:10.1175/1520-0442(2003)016, 2003.
- 1432 Taylor, K. E., Stouffer, R. J. and Meehl, G. A.: A Summary of the CMIP5 Experiment
1433 Design, 2009 ed., International CLIVAR Project Office. 2009.
- 1434 Tegen, I. and Fung, I.: Contribution to the Atmospheric Mineral Aerosol Load From
1435 Land-Surface Modification, *J Geophys Res-Atmos*, 100, 18707–18726, 1995.
- 1436 Thorndike, A. S., Rothrock, D. A., Maykut, G. A. and Colony, R.: The thickness
1437 distribution of sea ice, *J. Geophys. Res.*, 80(33), 4501–4513,
1438 doi:10.1029/JC080i033p04501, 1975.
- 1439 Valcke, S.: The OASIS3 coupler: a European climate modelling community software,
1440 *Geoscientific Model Development*, 6(2), 373–388, doi:10.5194/gmd-6-373-2013,
1441 2013.
- 1442 Voldoire, A., Sanchez-Gomez, E., Salas y Méliá, D., Decharme, B., Cassou, C.,
1443 Sénési, S., Valcke, S., Beau, I., Alias, A., Chevallier, M., Déqué, M., Deshayes, J.,
1444 Douville, H., Fernandez, E., Madec, G., Maisonnave, E., Moine, M. P., Planton, S.,
1445 Saint-Martin, D., Szopa, S., Tyteca, S., Alkama, R., Belamari, S., Braun, A., Coquart,
1446 L. and Chauvin, F.: The CNRM-CM5.1 global climate model: description and basic
1447 evaluation, *Climate Dynamics*, 40(9-10), 2091–2121, doi:10.1007/s00382-011-1259-
1448 y, 2013.
- 1449 Wanninkhof, R.: A relationship between wind speed and gas exchange over the ocean,
1450 *J. Geophys. Res.*, 97(C5), 7373–7382, 1992.
- 1451 Wanninkhof, R., Park, G.-H., Takahashi, T., Sweeney, C., Feely, R., Nojiri, Y.,
1452 Gruber, N., Doney, S. C., McKinley, G. A., Lenton, A., Le Quéré, C., Heinze, C.,
1453 Schwinger, J., Graven, H. and Khatiwala, S.: Global ocean carbon uptake: magnitude,
1454 variability and trends, *Biogeosciences*, 10(3), 1983–2000, doi:10.5194/bgd-9-10961-
1455 2012, 2013.
- 1456 Wassmann, P., Duarte, C. M., AGUSTÍ, S. and SEJR, M. K.: Footprints of climate
1457 change in the Arctic marine ecosystem, *Global Change Biol*, 17(2), 1235–1249,
1458 doi:10.1111/j.1365-2486.2010.02311.x, 2010.
- 1459 Watanabe, M., Kamae, Y., Yoshimori, M., Oka, A., Sato, M., Ishii, M., Mochizuki, T.
1460 and Kimoto, M.: Strengthening of ocean heat uptake efficiency associated with the
1461 recent climate hiatus, *Geophys. Res. Lett.*, 40(12), 3175–3179, doi:10.1002/grl.50541,
1462 2013.
- 1463 Wenzel, S., Cox, P. M., Eyring, V. and Friedlingstein, P.: Emergent constraints on
1464 climate-carbon cycle feedbacks in the CMIP5 Earth system models, *J. Geophys. Res.*
1465 *Biogeosci.*, 2013JG002591, doi:10.1002/2013JG002591, 2014.
- 1466 Wetzel, P., Maier-Reimer, E., Botzet, M., Jungclaus, J., Keenlyside, N. and Latif, M.:

1467 Effects of ocean biology on the penetrative radiation in a coupled climate model, ...
1468 of climate, 19(16), 3973–3988, 2006.

1469 Willis, J. K., Roemmich, D. and Cornuelle, B.: Interannual variability in upper ocean
1470 heat content, temperature, and thermosteric expansion on global scales, J. Geophys.
1471 Res., 109(C12), C12036, doi:10.1029/2003JC002260, 2004.

1472 [Yin, X.: Responses of leaf nitrogen concentration and specific leaf area to](#)
1473 [atmospheric CO2 enrichment: a retrospective synthesis across 62 species, Global](#)
1474 [Change Biol., 8\(7\), 631–642, doi:10.1046/j.1365-2486.2002.00497.x, 2002,](#)

1475 Zhu, Z., Bi, J., Pan, Y., Ganguly, S., Anav, A., Xu, L., Samanta, A., Piao, S., Nemani,
1476 R. and Myneni, R.: Global Data Sets of Vegetation Leaf Area Index (LAI)3g and
1477 Fraction of Photosynthetically Active Radiation (FPAR)3g Derived from Global
1478 Inventory Modeling and Mapping Studies (GIMMS) Normalized Difference
1479 Vegetation Index (NDVI3g) for the Period 1981 to 2011, Remote Sensing, 5(2), 927–
1480 948, doi:10.3390/rs5020927, 2013.

1481
1482
1483
1484
1485
1486
1487
1488
1489
1490
1491

roland seferian 26/2/16 16:54
Formatted: Font:12 pt

roland seferian 22/2/16 12:17
Formatted: Don't adjust space between Asian text and numbers

roland seferian 26/2/16 16:54
Formatted: Font:Not Bold

roland seferian 26/2/16 16:54
Formatted: Font:12 pt

roland seferian 26/2/16 16:54
Formatted: French

TOA	NSF	T _{2m}	SST	SWI	SSS	NIV	SIV	LCF	OCF
[W m ⁻²]	[W m ⁻²]	[°C]	[°C]	[-]	[psu]	[10 ³ km ³]	[10 ³ km ³]	[Pg C y ⁻¹]	[Pg C y ⁻¹]

Drift	4.4 10 ⁻⁴	4.5	-1.2	9.6 10 ⁻⁵	-1.6 10 ⁻⁵	-1.9 10 ⁻⁵	-4.4	7.2 10 ⁻³	-1.5	-2.0
[units century ⁻¹]		10 ⁻⁴	10 ⁻⁵				10 ⁻³	10 ⁻³	10 ⁻⁴	10 ⁻⁴

1492 **Table 1:** Drift in climate indices used to evaluate the equilibrium of CNRM-ESM1's
1493 physical and biogeochemical components. The drifts are computed over the 250-year
1494 long preindustrial simulation of CNRM-ESM1 for the top of the atmosphere net
1495 radiative balance (TOA), the net surface heat flux (NSF), the near-surface temperature
1496 (T_{2m}), the sea surface temperature (SST), the sea surface salinity (SSS), the soil
1497 wetness index (SWI), the northern and southern sea-ice volume (NIV and SIV,
1498 respectively) as well as the land and ocean global carbon fluxes (LCF and OCF).

1499

1500

1501

Regions	CNRM-ESM1	MTE-FluxNet	CNRM-ESM1	MTE-FluxNet
	GPP [Pg C y ⁻¹]		TER [Pg C y ⁻¹]	
High latitude north (>60°N)	2.6	4.8±0.8	2.5 (38%)	3.1±0.8
Mid-latitude North (20°N- 60°N)	37.9	34.8±2.7	36.23 (52%)	29.9±2.7
Tropics (20°S- 20°N)	73.2	62.3±1.9	72.58 (72%)	54.8±1.9
Mid-latitude South (20°S- 60°S)	16.1	9.3±0.6	15.6 (56%)	8.5±0.6
Global	130.0	111.3±6.0	126.9 (64%)	96.4±6.0

1502 **Table 2:** Regional and global budget of gross primary production (GPP) and
1503 terrestrial ecosystem respiration (TER) as simulated by the CNRM-ESM1 and

1504 | estimated from the FluxNet-MTE data product. Values in brackets indicate the ratio
 1505 | between the autotrophic respiration (Ra) and TER. The uncertainties for the FluxNet-
 1506 | MTE data product derives from the regional partitioning of global mean uncertainties
 1507 | published in (Jung et al., 2011). GPP and TER fluxes are determined from a yearly
 1508 | average over 1986-2005.

roland seferian 2/12/15 18:06
 Deleted: values

1509

1510

		CNRM-ESM1	Observations
T _{2m} [°C]	mean	0.43	0.30±0.08 (Morice et al., 2012)
	IAV	0.13	0.10
	trend	4.0 10 ⁻²	2.6 10 ⁻²
SIE [10 ⁶ km ²]	mean	4.68	6.70±0.26 (Comiso, 1999; Fetterer et al., 2002; Rayner et al., 2003)
	IAV	1.14	0.46
	decadal	-16 10 ⁻²	-6.8 10 ⁻²
OHC [10 ²² J]	mean	3.34	3.50±1.42 (Levitus et al., 2012)
	IAV	0.69	1.43
	trend	0.44	0.50
LCS [Pg C y ⁻¹]	mean	2.19	2.06±1.0 [models] (Le Quéré et al., 2014) 2.19±0.8 [Residual land carbon sink] (Friedlingstein et al., 2010)
	IAV	0.59	1.01
	trend	0.3 10 ⁻²	1.8 10 ⁻²
	mean	1.65	1.87±0.4 [models] (Le Quéré et al., 2014) 2.15±0.5 [obs.-models combination] 2.0±0.7 (Takahashi et al., 2010)

OCS [Pg C y ⁻¹]	IAV	0.09	0.14
	trend	4.5 10 ⁻²	1.8 10 ⁻²

1511 **Table 3:** Modern mean-state, interannual variability (IAV) and decadal trends of
1512 various global climate indices: the near-surface temperature (T_{2m}), Arctic September
1513 sea-ice extent (SIE), 0-2000m ocean heat content (OHC) as well as the land and ocean
1514 carbon sinks (LCS and OCS respectively). For LCS and OCS, positive values indicate
1515 an uptake of CO₂ by land and ocean. All metrics are computed over the 1986-2005
1516 period for both model and observations. Decadal trends are estimated from linear
1517 regression over the 1986-2005 period. IAV is estimated from the standard deviation of
1518 the detrended time series.

1519

1520

1521

1522

1523 **Figure 1:** Fraction of dominant vegetation type as prescribed in SURFEX. This
1524 fraction results from aggregation of the various ECOCLIMAP's vegetation types at 1
1525 km resolution over the T127 CNRM-ESM1 horizontal grid (~1.4° nominal horizontal
1526 resolution).

1527

1528 **Figure 2:** Time series of various climate indices along the 250-year long control
1529 simulation. (a) Net radiative fluxes at the top of the atmosphere (in red, left y-axis)
1530 and surface (in blue, right y-axis) are used to assess the stability of the climate energy
1531 flow in the model; (b) Near-surface global average temperature (in red, left y-axis)
1532 and global averaged sea surface temperature (in blue, right y-axis); (c) Soil wetness
1533 index (in red, left y-axis) and sea surface salinity (in blue, right y-axis) are used as
1534 proxy of the hydrological cycle; (d) Sea ice volume in the Northern Hemisphere (in
1535 red, left y-axis) and in the Southern Hemisphere (in blue, right y-axis) are used to

1536 evaluate the stability of the cryosphere component in CNRM-ESM1; (e) Global
1537 carbon fluxes over land (in red, left y-axis) and over ocean (in blue, right y-axis) are
1538 used to assess the equilibration of the global carbon stock. For carbon fluxes, positive
1539 (negative) fluxes indicate an uptake (outgasing) of CO₂ by land or ocean.

1540

1541 **Figure 3:** Biases in simulated near-surface temperature (T_{2m}) compared to the
1542 CRUTV4 observations (Harris et al., 2013) averaged 1986-2005. Winter (a) and
1543 summer (b) periods are computed from DJFM and JJAS months.

1544

1545 **Figure 4:** Biases in simulated precipitation (PR) compared to the GPCP observations
1546 (Adler et al., 2003) averaged over 1986-2005. Winter (a) and summer (b) periods are
1547 computed from DJFM and JJAS months.

1548

1549 **Figure 5:** Biases in simulated photosynthetically available radiation (PAR) compared
1550 to the SRB satellite-derived observations (Pinker et al., 1992) averaged over 1986-
1551 2005. Winter (a) and summer (b) periods are computed from DJFM and JJAS months.

1552

1553 **Figure 6:** Annual bias patterns of simulated temperature T and salinity S averaged
1554 over 1986-2005 compared to the WOA2013 observations (Levitus et al., 2013).
1555 Surface biases for sea surface temperature (a) and salinity (b) are represented using
1556 the same colorbar. Vertical structure of biases for temperature (c) and salinity (d) are
1557 estimated using zonal-average biases from WOA2013 across the Atlantic and Pacific
1558 oceans.

1559

1560 **Figure 7:** Composite of yearly extremum of mixed-layer depth over 1986-2005. Left
1561 panels represent the maximum mixed-layer depth (MLD_{max}) for (a) observations

roland seferian 19/12/15 13:00

Deleted: -

1562 (Sallée et al., 2010) and (b) CNRM-ESM1. Right panels represent the minimum
1563 mixed-layer depth (MLD_{min}) for observations (c) and CNRM-ESM1 (d).

1564

1565 **Figure 8:** Sea ice cover (SIC) as simulated by CNRM-ESM1 averaged over 1986-
1566 2005. Top panels represent composite of September sea ice cover, while bottom
1567 panels are for March. Iso-15% of SIC serves as comparison between model results
1568 and NSIDC observations (Cavalieri et al., 1996) averaged over 1986-2005; model
1569 results and observations are indicated with dashed and solid black lines, respectively.

1570

1571 **Figure 9:** Taylor diagrams showing the correspondence between model results and
1572 observations for CNRM-ESM1 and CNRM-CM5.2. Near-surface temperature (T_{2m}),
1573 precipitation (PR) and incoming short-wave radiation (RSDS) are used to assess
1574 model performance over land surface. Sea surface temperature (SST), sea surface
1575 salinity (SSS), mixed-layer depth (MLD) and precipitation (PR) are used to assess
1576 model performance over ocean. Filled and empty symbols indicate skills for CNRM-
1577 ESM1 and CNRM-CM5.2, respectively. The size of the symbols indicates whether
1578 statistics were computed from annual mean climatology or seasonal average (JFM,
1579 AMJ, JAS, OND) over 1986-2005.

1580

1581 **Figure 10:** Impact of coupling frequency on sea ice cover (SIC) as simulated by
1582 CNRM-ESM1 averaged over 1986-2005. Top panels represent composite of
1583 September sea ice cover, while bottom panels are for March. Iso-15% of SIC serves
1584 as comparison between model results using a 6-h coupling frequency (dashed lines)
1585 and those using a 24-h coupling frequency (solid lines).

1586

1587 **Figure 11:** Annual-mean terrestrial gross primary production (GPP). Values are given
1588 for (a) observation-derived MTE-FluxNet (Jung et al., 2009) averaged over 1986-

roland seferian 2/12/15 12:46

Deleted: 0

1589 2005, (b) satellite-derived observation from MODIS over 2000-2013 and (c) CNRM-
1590 ESM1 over 1986-2005.

1591

1592 | **Figure 12:** Annual-mean autotrophic respiration (R_a) as estimated from MODIS over
1593 2000-2013 (a) and as simulated by CNRM-ESM1 (b) over 1986-2005. Panel (c)
1594 represents the zonal-cumulated R_a in function of latitude for both satellite-derived
1595 estimates (in blue) and CNRM-ESM1 (in red).

roland seferian 2/12/15 12:46

Deleted: 1

1596

1597 | **Figure 13:** Stocks of modern soil organic carbon (c_{Soil}) as estimated from
1598 FAO/IIASA/ISRIC/ISSCAS/JRC (2012) Harmonized World Soil Database (a) and as
1599 simulated by CNRM-ESM1 (b) averaged over 1986-2005. Panel (c) represents the
1600 zonally-cumulated soil organic stock in function of latitude for both observation-
1601 based estimates (in blue) and CNRM-ESM1 (in red).

roland seferian 2/12/15 12:46

Deleted: 2

1602

1603 | **Figure 14:** Taylor diagrams showing the correspondence between model results and
1604 observations for CNRM-ESM1 and CNRM-CM5.2 (Séférian et al., 2013).
1605 Climatological distribution over 1986-2005 of simulated Oxygen (O_2), phosphate
1606 (PO_4), nitrate (NO_3) and silicate (SiO_2) concentrations are assessed against WOA2013
1607 data product. Filled and empty symbols indicate skills for CNRM-ESM1 and CNRM-
1608 CM5, respectively. The size of the symbols indicates the depth at which statistics have
1609 been computed.

roland seferian 2/12/15 12:46

Deleted: 3

1610

1611 | **Figure 15:** Annual-mean ocean carbon fluxes ($fgCO_2$) as estimated by the Takahashi
1612 et al., (2010) database (a) and as simulated by CNRM-ESM1 averaged over 1986-
1613 2005 (b). Panel (c) represents the zonal-cumulated carbon fluxes in function of
1614 latitude for both observation-based estimates (in blue) and CNRM-ESM1 (in red).
1615 Negative (positive) fluxes indicate an uptake (outgasing) of CO_2 .

roland seferian 2/12/15 12:46

Deleted: 4

1616

1617 | **Figure 16:** Annual-mean zonal-average anthropogenic carbon ($\text{CO}_2^{\text{ANTH}}$) across the
1618 Atlantic and Pacific oceans as simulated by CNRM-ESM1 averaged over 1990-2005
1619 (a) and as estimated from the GLODAP database compiling data up to 1994 (b). Panel
1620 (c) represents the mean-annual bias in zonal structures between model and
1621 observation-based estimates in $\text{CO}_2^{\text{ANTH}}$.

roland seferian 2/12/15 12:46

Deleted: 5

1622

1623 | **Figure 17:** Composite of yearly maximum of leaf area index (LAI_{max}) as estimated
1624 from AVHRR satellite observations of Zhu et al. (2013) (a) and as simulated by
1625 CNRM-ESM1 (b) over 1986-2005. Panel (c) represents the zonal-average LAI_{max} in
1626 function of latitude for both observation-based estimates (in blue) and CNRM-ESM1
1627 (in red).

roland seferian 2/12/15 12:46

Deleted: 6

1628

1629 | **Figure 18:** Annual-mean surface chlorophyll concentrations (Chl) as estimated from
1630 SeaWiFS over 1997-2010 (a) and as simulated by CNRM-ESM1 (b) over 1986-2005.
1631 Panel (c) represents the zonal-averaged Chl in function of latitude for both satellite-
1632 derived estimates (in blue) and CNRM-ESM1 (in red).

roland seferian 2/12/15 12:46

Deleted: 7

1633

1634 | **Figure 19:** Time series of various climate indices as monitored from available
1635 observations (blue solid line) and as simulated by CNRM-ESM1 (red solid line) since
1636 1901 with global near-surface temperature (a), September arctic sea-ice extent (b), 0-
1637 2000m ocean heat content (c), land carbon flux (d) and ocean carbon flux (e).
1638 Hatching represents the $\pm 2\sigma$ estimated from the ensemble deviation between the 100
1639 members of the HadCRUT4 database (Morice et al., 2012) for near-surface
1640 temperature, the standard deviation between NSIDC Fetterer et al. (2002), Comiso
1641 (1999) and Hadisst (Rayner et al., 2003) databases, the pentadal variability of the
1642 observed ocean heat content (Levitus et al., 2012) and spread between Global Carbon
1643 Project reconstructions for both land and ocean (Le Quéré et al., 2014). For both OCS
1644 and LCS, positive (negative) fluxes indicate an uptake (outgasing) of CO_2 .

roland seferian 2/12/15 12:46

Deleted: 8

1645

1646 **Figure 20:** Skill-score matrix based on (a) spatial correlation and (b) globally
1647 averaged root-mean squared error for relevant fields of the simulated carbon cycle
1648 from current generation Earth System models. Leaf area index (LAI), gross primary
1649 productivity (GPP), autotrophic respiration (Ra), heterotrophic respiration (Rh) and
1650 soil carbon (cSoil) are used to assess model skill in terms of modern mean-state
1651 terrestrial carbon cycle. Sea-air carbon flux (f_{gCO_2}), surface chlorophyll (Chl) and
1652 surface concentrations of oxygen (O_2), nitrate (NO_3), phosphate (PO_4) and silicon (Si)
1653 are used to evaluate the skill of the current models at replicate modern mean-state
1654 ocean carbon cycle. Both models and observed fields are averaged over time from
1655 1986 to 2005 to determine skill score metrics, except for cSoil, O_2 , NO_3 , PO_4 , Si
1656 observations (only a modern mean-state climatology is available). Black squares
1657 indicate that models fields are not available (implying that these fields are either not
1658 simulated by the model or not published on the ESGF).

roland seferian 20/2/16 22:50

Formatted: Subscript

roland seferian 20/2/16 22:50

Formatted: Subscript

roland seferian 20/2/16 22:50

Formatted: Subscript

roland seferian 20/2/16 22:50

Formatted: Subscript